FUNDAMENTALS AND PRACTICAL APPROACHES OF OPTIMIZING MARTENSITIC STEELS FOR USE UNDER SEVERE OPERATING CONDITIONS

H. Mohrbacher[1], J.W. Morris[2] and G. Krauss[3]

[1]NiobelCon bvba, 2970 Schilde, Belgium
[2]University Emeritus Professor, University of California, Berkeley, CA 94720, USA
[3]University Emeritus Professor, Colorado School of Mines, Golden, CO 80401, USA

Keywords: Martensite, Effective Grain Size, Fracture Modes, Embrittlement, Tempering, Reheat Quenching, Direct Quenching, Case Carburizing, Precipitates, Niobium, Molybdenum

Abstract

Martensitic steel is a well-established material for the equipment and tooling used in mining and processing. Martensitic steel was originally chosen for its high strength and hardness. However, the overall performance of industrial machinery requires that a number of other properties be considered, including toughness, ductile-to-brittle transition temperature, fatigue strength, resistance to temper and hydrogen embrittlement, corrosion, creep, abrasion resistance, bendability (cold forming), and machinability. Often, a number of these properties should be optimized simultaneously. This optimization is achieved by adjusting alloy composition or thermomechanical processing, or ideally, by a well balanced combination of both. A clear understanding of the microstructure of martensitic steel and how it governs properties must precede any optimization exercise. Accordingly, we begin by outlining some fundamental considerations concerning the microstructure of martensite and its influence on strength, toughness and failure mechanisms. Next, we discuss the role of the various alloying elements and typical impurities on the microstructure and, hence the relevant properties. Typical alloying elements such as carbon, molybdenum, niobium, chromium, manganese and boron not only have primary effects, but also have cross-effects and synergies when added in combination. Thirdly, we describe the variety of thermomechanical processes that make it possible to tailor properties to a particular performance profile. These span the range from traditional quench-and-temper (Q&T) treatments to more recent processes, such as direct quenching, quench-and-partition and intercritical heat treatments. Each step of each treatment must be analyzed for its influence on the final microstructure and thus, the ultimate combination of properties. Finally, we present specific examples of technologically successful martensitic steels. We describe their composition and processing, particularly focusing on the effects and benefits of niobium and molybdenum as alloying elements.

Introduction

As-quenched martensite is the hardest and strongest microstructure of carbon steel. After tempering it produces many excellent combinations of properties making it suitable for a wide variety of demanding applications. Particularly for applications in the mining and processing industry, hardness and strength are fundamental assets providing good functionality and sufficiently long life of components under severe service conditions. Thereby, hardness is associated with resistance against wear in general and abrasion in particular. High strength allows sustaining high loads and forces without having to design components of excessively heavy gage, thus reducing their weight and dimensions. Beyond that fundamental aspect, a wide range of severe operating conditions exist requiring additional properties and characteristics that have to be implemented into martensitic steels. In many applications components are subjected to high impact loads. Accordingly, toughness and ductile-to-brittle transition behavior have to be considered, the latter being particularly important when operations are taking place in cold climate conditions. In many applications the steel is in contact with aggressive media, such as acids, bases or seawater. Thus, corrosion resistance of the material is an important aspect. Since corrosion reactions typically also serve as a source of generating free hydrogen, resistance against hydrogen embrittlement and delayed cracking needs to be considered as well. Other applications take place in hot environments requiring resistance against tempering and creep, heat conduction, as well as resistance against thermal fatigue and oxidation. It is quite obvious that there is no ideal material fulfilling all these requirements in an optimum way. Besides, such a widely performing material would be too expensive for most of the simpler application profiles. Therefore, the steel has to be tailor-made to the application concerning design of its microstructure, as well as alloy concept.

The microstructure is adjusted by modification of the alloy concept and processing route. Consequently, the present paper initially analyzes how features of the martensitic microstructure relate to properties. Subsequently, the effects of various alloying elements relevant to martensitic steels will be considered. Inherently, these alloy effects have also to be seen in the light of the processing route chosen to produce the steel. Thus, customary processes such as reheat quenching, direct quenching and case carburizing are addressed. On that basis of understanding, practical approaches of optimizing martensitic steel will be discussed, thereby particularly focusing on the effects and benefits of niobium and molybdenum as alloying elements.

Microstructure and Properties

General Considerations

Martensite, being the hardest microstructural variant of steel, is formed from austenite when the cooling speed is fast enough to prevent diffusion-controlled transformation. The hardness (and thus strength) of fully quenched martensite increases nearly linearly with the carbon content over the range of 0 to 0.5%C, Figure 1 [1]. Simultaneously, the start temperature of martensite transformation decreases with increasing carbon content from around 550 °C for very low carbon content to below 350 °C when approaching 0.5% carbon. Therefore, the lower the carbon content, the more prominent self-tempering effects become under industrial quenching conditions. In as-quenched martensite, carbon atoms, either trapped in octahedral interstitial sites

of the body-centered-tetragonal lattice, or segregated to dislocations or interfaces, dominate the strengthening mechanism.

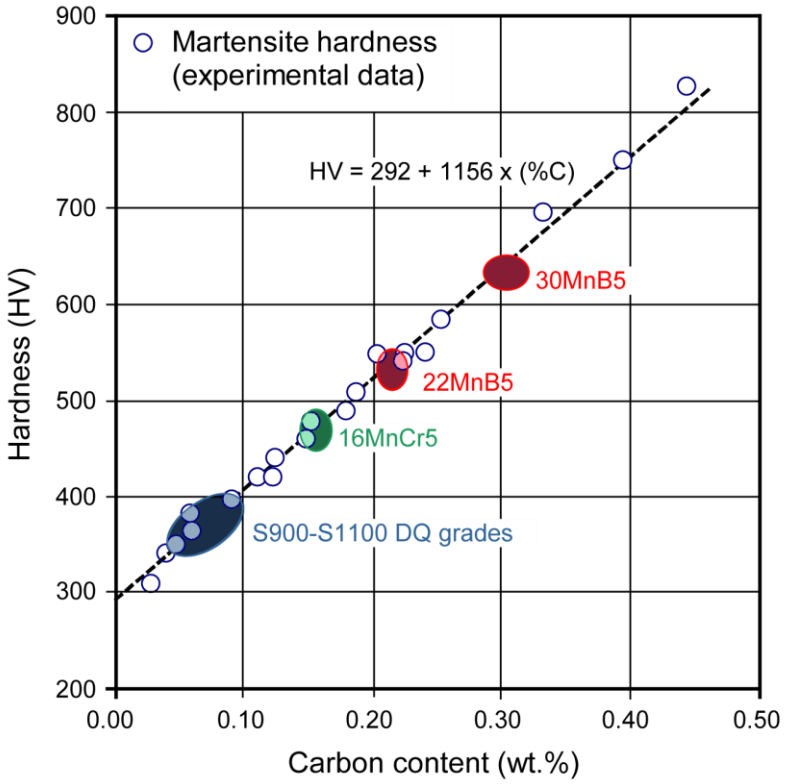

Figure 1. Correlation between carbon content and as-quenched martensite hardness (indication of commercialized grades).

Steels are often divided into three categories based on their carbon content. Low-carbon steels have carbon contents remaining below 0.2%. Medium-carbon steels have carbon contents between 0.2 and 0.5% and high-carbon steels have carbon contents above 0.5%. Although this classification may appear arbitrary at first sight, there are sound metallurgical arguments justifying it. At carbon concentrations below 0.2%, about 90% of the solute carbon atoms segregate to dislocations during the quenching process, Figure 2. Above 0.20% these defect sites become almost saturated and carbon atoms remain in octahedral interstitial sites [2]. Unless the rate of cooling during quenching is increased greatly, 0.2%C is also the point at which the martensite crystal becomes measurably tetragonal. The boundary between medium- and high-carbon steels is considered to be at 0.50%C because above this level steels become susceptible to intergranular fracture in the as-quenched and quenched-and-low-temperature-tempered conditions [3]. Furthermore, quenched steel containing carbon higher than 0.5% forms more complicated microstructures, as lath martensite is gradually replaced by plate martensite and the fraction of retained austenite increases.

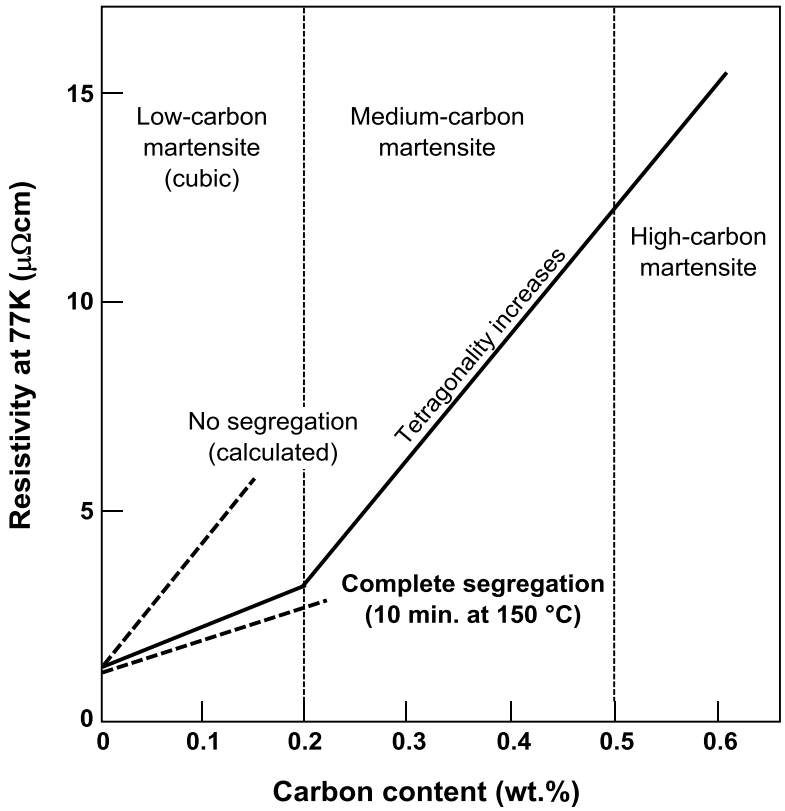

Figure 2. Carbon segregation during quenching of iron-carbon martensites measured by electrical resistivity (adapted from G.R. Speich [2]).

Low- and medium-carbon steels are the types most commonly used in the mining and processing industry. Low-carbon steels are often used in the as-quenched (optionally tempered) condition for structural applications requiring strength in the range 900 to 1400 MPa. Medium-carbon steels are widely used in the quench and tempered condition. These serve, for instance, in abrasive resistant applications, tools and dies for material processing, power transmission units, seamless pipes and ballistic plates. Since these are all lath martensitic steels, the microstructural features of lath martensites, their relationship to properties, and the effect of various tempering treatments will be discussed in some detail in the following section.

Microstructural Characteristics of Lath Martensite

In low- and medium-carbon steels the martensite microstructure consists of laths that are grouped into blocks and subsequently, into packets, Figure 3. The laths are highly dislocated. The crystal structure of low-carbon lath martensite is body centred cubic (bcc), but at carbon contents in excess of 0.20% the structure becomes slightly tetragonal.

To understand the basic microstructure of low-carbon lath martensitic steel, it is important to recognize two basic crystallographic relations between the parent face centred cubic (fcc) austenite and the product bcc ferrite [4,5]. Firstly, the two crystal structures are connected by the "Bain strain", the bcc unit cell is derived from fcc by compressing the fcc cell along one of the

<100>$_\gamma$ cube axes, while expanding it homogeneously in the perpendicular plane. There are hence three "Bain variants" of the transformation, corresponding to the three possible choices of the compression axis. Secondly, after transformation, the crystal axes of the martensite laths are oriented in (or very close to) the Kurdjumov-Sachs (KS) orientation relations, with the close-packed planes and close-packed directions of the bcc product parallel to those of the fcc parent: {110}$_\alpha$||{111}$_\gamma$, <111>$_\alpha$||<110>$_\gamma$.

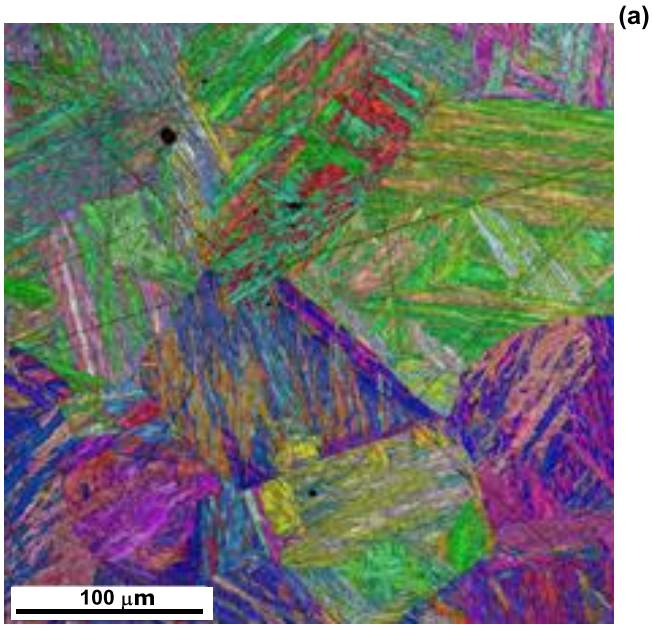

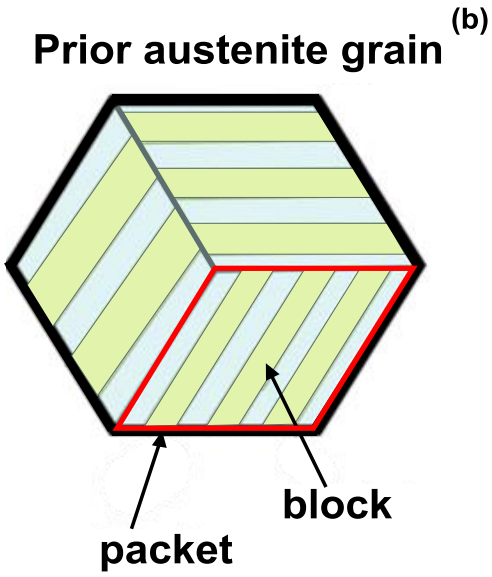

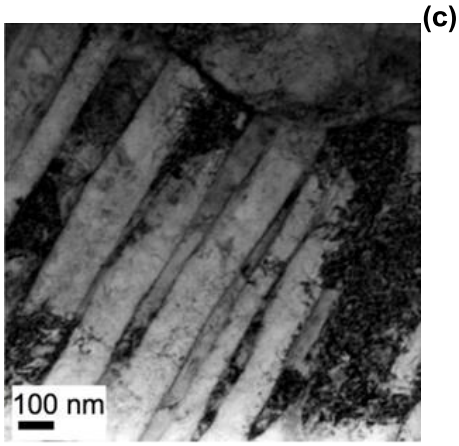

Figure 3. Martensitic substructure within a prior austenite grain of low-carbon steel;
(a) EBSD map of prior austenite grains [5], (b) Schematic drawing showing packets and blocks,
(c) TEM micrograph showing laths within a block.
(TEM micrograph courtesy of J.R. Yang, National Taiwan University).

There are four independent choices for the $\{111\}_\gamma$ plane and for each choice of $\{111\}_\gamma$, there are six independent ways to choose the bcc close-packed plane and direction to satisfy the KS relations. These are illustrated in Figure 4. It follows that there are 24 "KS variants" of the transformation. Eight of these, two per choice of $\{111\}_\gamma$, are examples of each of the three Bain variants of the transformation.

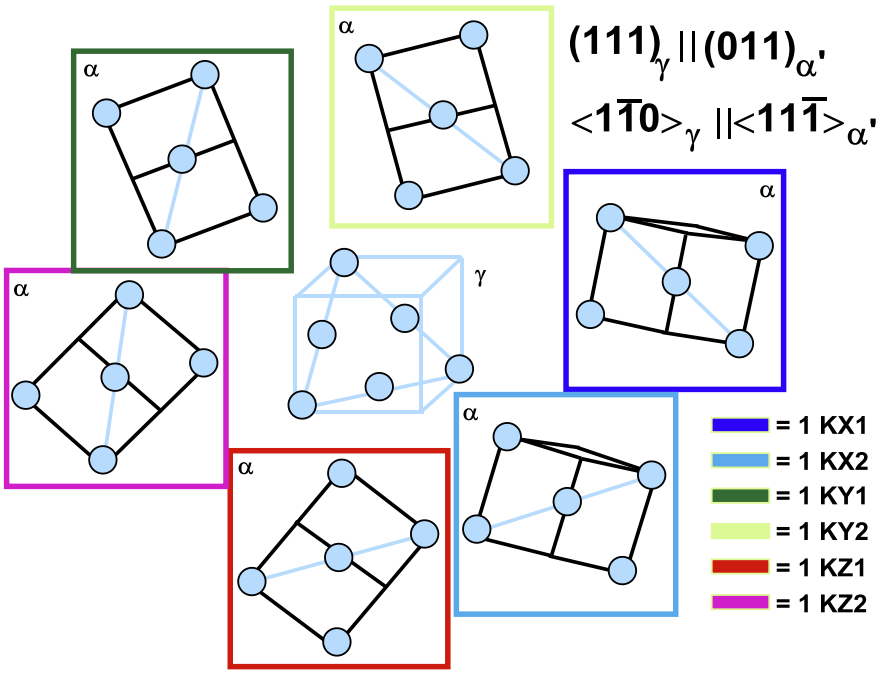

Figure 4. The six crystallographic variants of bcc that satisfy the KS relation on $(111)_\gamma$. Variants of the same color (red, blue, green) have the same Bain axis. Variants that share the same close-packed direction are twinned with respect to one another. Variants colored dark (light) are rotated 120° from one another in the plane.

In the basic microstructure of lath martensitic steel [5-8] each prior austenite grain is subdivided into packets, Figure 3. There are four crystallographically distinct packets, each based on one of the four choices of $\{111\}\gamma$ plane. Each packet is a composite of laths that have one of the six KS relations that share the $\{111\}\gamma$ plane of the packet. The packet is then subdivided into "blocks" which are plates with $\{110\}\alpha$ habit planes that are stacked to fill the packet. Each block is a composite of two "sub-blocks," each of which is built up of laths from one of the two KS variants that belong to the packet and have the same Bain axis, Figure 4. The final structure is shown in Figure 3(a) and, schematically, in Figure 3(b).

While this highly organized structure may seem complex, it actually has a fairly simple interpretation [9,10]. Given the large strain involved in the fcc-bcc transformation, there must be an efficient way to accommodate this strain for the transformation to happen at all and there must be an efficient way to relax the overall strain to prevent "quench cracking" as the transformation proceeds. It can be shown [10] that, with a suitable choice of slip systems, a composite plate (block) made up of two KS variants from the same packet with the same Bain axis has an invariant plane with the fcc parent that parallels the common $\{110\}\alpha$ plane ($=\{111\}\gamma$ plane) of the packet. It follows that the six KS variants within a given packet can be gathered into parallel plates (blocks) of three distinct types, and these can simply be stacked to fill space. If the volume fractions of the three blocks are the same, the only residual shear strain is due to a linear expansion perpendicular to the plates. If all four distinct blocks appear with similar volume fractions in a prior austenite grain, the four linear expansions balance, and the net strain of the whole grain is a simple dilatation; the transformation shear is fully relaxed. Given this microstructural pattern, a polygranular austenite can transform martensitically to a polygranular product with little or no residual shear strain.

This microstructural pattern has several important consequences, including: (1) while the individual blocks are composites of two KS variants, the boundary between them is a low-angle boundary. Since the boundaries between the individual laths in the block are even smaller, the blocks behave essentially as single crystals, as has long been observed [9]. (2) The boundaries between blocks that have different Bain variants are high-angle boundaries, but the angles have one of a few discrete values, as observed [6,8]. (3) Given the need to minimize elastic energy, the same microstructural pattern is favored for all prior austenite grains of reasonable size. It follows that the block and packet sizes tend to scale linearly with the prior austenite grain size (PAGS) until the grain size becomes so small that surface effects become dominant, as observed [7].

The dislocated lath microstructure described here is found generally in low-carbon martensites, excepting the very finest prior austenite grain sizes, where boundary effects become important. The microstructural pattern becomes less regular at higher carbon contents, due to a combination of carbon-induced tetragonality and carbon redistribution during the transformation. In high-strength, medium carbon steels such as AISI 4140 there is a significant population of single-variant blocks with lath and block boundaries sheathed in retained austenite or precipitated carbide.

The Effective Grain Size

Many important properties of polycrystalline materials are related to the grain size. Smaller grain size in ferritic steels increases strength and toughness and simultaneously it lowers the ductile-to-brittle transition temperature, according to Hall-Petch type relationships. In polygonal ferritic steels, the grain size can easily be determined by light optical microscopy. In martensite, however, determination of the grain size is not trivial and requires more sophisticated microstructural analysis tools, such as EBSD and TEM. Yet, the initial question that needs to be answered is: *"which is the relevant definition of grain size in martensitic steel?"* Morris and co-workers [9] have approached this question by defining an "effective grain" size in martensite that may be different for the various properties. Strength, cleavage resistance, and ductile–brittle transition temperature are related to the effective grain size (d_{eff}) as follows:

The yield strength (σ_y) is given by the classic Hall–Petch relationship:

$$\sigma_y = \sigma_0 + K_y d_{eff}^{-1/2} \tag{1}$$

where K_y is the Hall–Petch coefficient for strength. σ_0 is a material constant for the starting stress for dislocation movement.

The cleavage fracture stress (σ_f) obeys a relationship of the form:

$$\sigma_f = K_f d_{eff}^{-1/2} \tag{2}$$

where K_f is the Hall–Petch coefficient for cleavage.

The ductile–brittle transition temperature often obeys a constitutive equation of the form:

$$T_B = T_0 - K_B d_{eff}^{-1/2} \tag{3}$$

where K_B is the appropriate Hall–Petch coefficient. T_0 is the temperature at which yield strength becomes equal to the cleavage stress.

It is important to recognize that "grain size" has a different meaning for each of the properties of interest.

Maki et al. [7] analyzed correlations of substructure size and parent austenite size in some detail. As expected, the packet size decreases as the prior austenite grain size decreases. Larger austenite grains transform into a substructure consisting of several packets. For a prior austenite grain size finer than 10 μm, the packet size approaches that of the austenite grain size. By further refinement, it is possible that some prior austenite grains consist of a single packet (or even a single block). However, the effect of prior austenite grain size on the lath width is small.

Effective Grain Size for Strength

Early work by Cohen [11,12] found the yield strength of carbon-free martensite to be inversely proportional to the square root of the parent austenite grain size. The constant of proportionality in this Hall-Petch type relationship is such that a decrease in prior austenite grain size from 1 mm to 10 μm would raise the yield stress of the corresponding martensite by approximately 420 MPa. By extrapolating this relationship to $d^{-1/2} = 0$, a value for the yield strength of a hypothetical single crystal of martensite is obtained; this value is roughly 350 MPa. For an austenite grain size in the region of 50 μm, a yield strength of approximately 690 MPa is obtained. The total contribution due to grain size is therefore 340 MPa. If it is now assumed that the addition of carbon to martensite alters the σ_0 term, but not the constant K_y in Equation 1 (an assumption that is valid in the case of ferrites), it becomes apparent that the grain size contribution to the strength of high yield stress martensite is relatively small.

Later work on Fe-0.20C-Ni-Cr-Mo steel considered the packet size as the effective grain size for lath martensite [13]. This correlation was well supported by Wang et al. [14] on similar steel. When the prior austenite grain size in 17CrNiMo6 steel was refined from 199 μm to 6 μm, the yield strength increased by 235 MPa (representing a 25% increase), indicating that grain refinement is not very effective in increasing the strength. The work also demonstrated an almost equally good correlation between yield strength and the inverse square root of either packet size or prior austenite grain size, respectively (which is expected if the two microstructural measures scale together).

Recent work by Morito and Obha [15] showed that the replacement of packet size by block size in the Hall-Petch relationship for Fe-0.2%C and Fe-0.2%C-2%Mn steels produced a more consistent value of the Hall-Petch coefficient, and in fact, a value that is reasonably close to that found in ferritic Fe–Mn and in pure Fe, where the grain size is more easily defined. Lath size may be expected to have little effect on strength as there is little crystallographic distinction between adjacent laths, indeed *in situ* indentation studies [16] have demonstrated that the lath boundary presents almost no barrier to dislocations in the absence of boundary films.

In a review article, Morris [17] also argued that the block size is the effective grain size for strength. While it may seem obvious that the block size should be the effective grain size for strength, since it provides the smallest significant crystallographic discontinuity, a closer examination shows that the role of the block boundary involves some subtlety, particularly when the blocks are used to subdivide a prior austenite grain that is much larger in size. The first issue is topological. Crystallographically distinct blocks are different Bain variants of the parent austenite. Since there are only three of these, it is geometrically impossible to design a microstructure in which each block is surrounded by dissimilar neighbors. The effective grain size of lath martensitic steel is always some multiple of the block size.

The second issue is physical, and concerns whether a block boundary is an effective barrier to the transmission of plastic deformation [16,18,19]. The problem is that the Bain variants share common slip planes and hence, may not effectively inhibit slip. The experimental evidence on this issue is ambiguous and puzzling. For example, intercritical heat treatments used to refine the effective block size in lath martensitic steels show very little effect on the yield strength. On the

other hand, others [15] have found a strong Hall-Petch strengthening from block boundaries, comparable to that associated with high-angle boundaries generated by powder processing or incoherent transformations. A plausible explanation for this inconsistent behavior is found in the recent work of Ohmura and Tsuzaki [19] who combined nano- and micro-indentation to compare the intragranular and polygranular hardnesses of martensitic steels. Their data appears to show that strengthening by block or packet boundaries (ie. by Bain variant boundaries) is largely due to boundary decoration by carbon or carbide films. Their results may provide the key to understanding the influence of block size on strength. Decorated block boundaries strengthen much as incoherent boundaries do, while the relatively clean boundaries in low-carbon, gettered or tempered martensites have a much smaller effect on the strength.

Effective Grain Size for Toughness

Two fracture modes, quasi-cleavage and ductile fracture, were observed by Irani [20] in an early study on the fracture behavior of martensitic steel. In an impact test, the former is expected to absorb a lesser amount of energy than the latter. This correlation has been confirmed, as the absorbed impact energy increases with the amount of ductile fracture. Quasi-cleavage proceeds by the nucleation and growth of submerged cracks ahead of the advancing fracture front. The crack front advances in a stepwise manner as the cracks in front of the fracture tip grow until coalescence takes place, Figure 5. The advance of a quasi-cleavage fracture crack through a martensitic structure is transgranular with respect to the prior austenite grains. The quasi-cleavage fracture surface shows fractures characteristic of both true cleavage and plastic rupture. Firstly, extensive flat facets are seen on the fracture surfaces indicating true crystalline cleavage. This also holds for the formation of steps (S) during the growth of the facet. Secondly, tear ridges (T) are observed on fractographs. These are formed during the linking up of micro-cracks with the advancing fracture front. In this respect, quasi-cleavage resembles plastic rupture.

Naylor et al. [21,22] pointed out that micro-cracks formed within laths are too small to start cleavage due to the limited lath width. Micro-cracks in adjacent laths must join together to create a crack of critical length to propagate as cleavage. This crack experiences small deflections when crossing lath or sub-block boundaries and larger deflections when passing block boundaries, where they are often arrested. The blocks are thought to coincide with the facets seen in fractography.

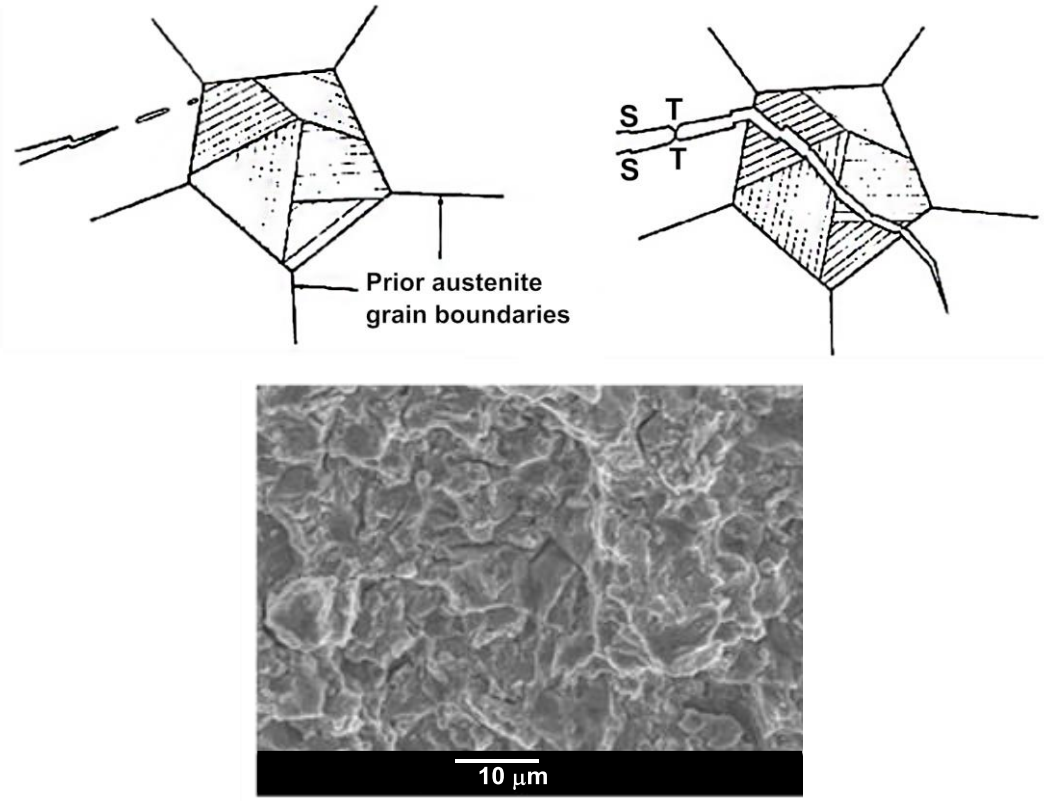

Figure 5. Schematic crack propagation with formation of steps (S) and tear ridges (T) and appearance of quasi cleavage fracture.

The microstructural mechanism of cleavage in ferritic steels is well known; ferritic steels cleave along {100} planes. It follows that, in the case of lath martensitic steels, the effective grain size is the coherence length on {100} planes, which determines the cleavage crack length. The {100} coherence length is fixed by the "block" size, which is the basic crystallographic unit. Refining the block size of martensitic steel is hence an effective means of increasing its resistance to transgranular cleavage fracture, since Bain variant boundaries are crystallographic discontinuities in the {100} cleavage planes. Consequently, block refinement is a very successful approach to lower the ductile-brittle transition temperature (DBTT) of steel whose transition is governed by transgranular cleavage. Morris et al. [23] used profile fractography and EBSD to show the specific role of block boundaries in arresting cleavage cracks in 9%Ni steel.

In similar work, results reported by Wang et al., [14] on 17CrNiMo6 steel demonstrated a marked increase of toughness at 77 K when the packet size becomes smaller than 10 μm. It is worth noting that the packet size effect on toughness was much larger than that on yield strength. The same authors [24] used EBSD techniques to show the boundary-induced decrease in cleavage crack length with block refinement in lath martensitic steel. Hanamura et al., [25] obtained similar results, but with less definitive microstructure characterization. Ishikawa et al., [26] analyzed the fracture behavior of 0.15%C abrasive resistant steel treated to 420 HV hardness. Charpy tests conducted at -196 °C revealed a relatively straight crack path for a conventional Q&T steel, while that of an ausformed steel (niobium microalloying + TMCP)

showed a much more corrugated crack path. This was due to many deflections at packet boundaries leading to higher energy consumption (the fracture mode still being brittle in both materials). Charpy tests performed at -40 °C indicated a marked increase in energy consumption when the prior austenite grain size was reduced to below 30 µm. The fracture appearance was becoming increasingly ductile at smaller prior austenite grain sizes.

The dimpled topography of ductile fracture is due to the concave depressions formed by the growth and coalescence of spherical micro-voids with the advancing crack front, Figure 6. These micro-voids may be nucleated at any heterogeneity, hence, the size and distribution of heterogeneities have an important influence on the formation, growth and coalescence of voids. The size to which a micro-void can grow depends partly on the work hardened state of the matrix, and thus the number of voids required for the propagation of a fracture front will increase with an increase in the work hardened condition of the matrix. Improving the cleanness of steel is an important means of increasing energy absorption in ductile fracture mode. In very clean steels voids can be generated at grain corners, setting the limit to this means of improvement.

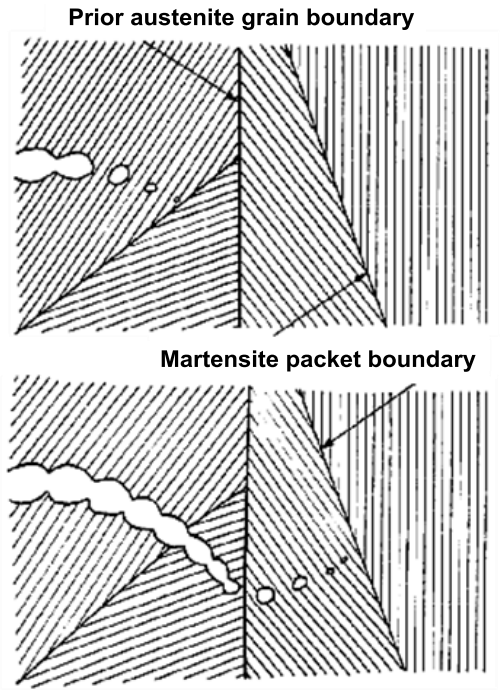

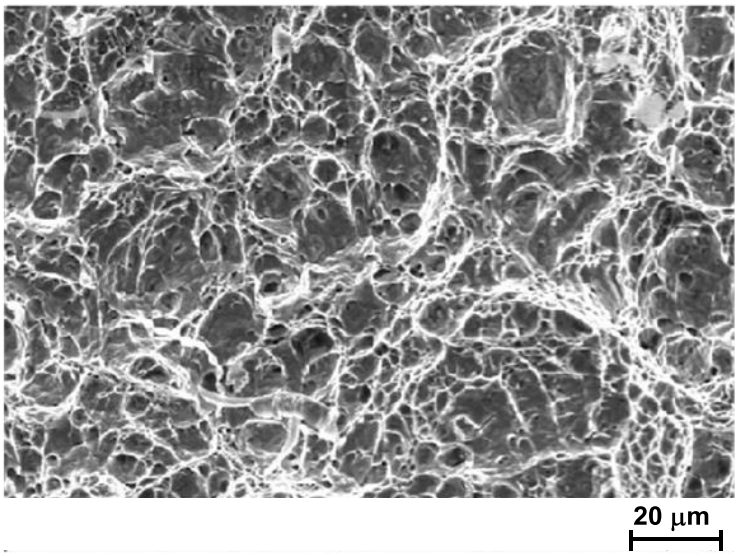

Figure 6. Schematic crack propagation and appearance of ductile fracture.

Lowering the Ductile-to-Brittle Transition Temperature

In ferritic steel the ductile-to-brittle transition temperature, T_B, can be efficiently lowered by reducing the carbon content and refining the grain size. Grain refinement compensates the loss of strength originating from the carbon reduction. This principle has found its culmination in modern TMCP steels.

In martensitic steel the transition temperature from a ductile dimple-type fracture to brittle cleavage-type fracture depends on the block size and the hardness (strength). Reducing carbon is not always an option as carbon is needed for strength and the trade-off with Hall-Petch strengthening from grain refinement may be insufficient. The linear correlation between the inverse square root of the packet size (hence, by inference, block size) and T_B according to Equation 3 was demonstrated for different alloys [27]. The Hall-Petch coefficient K_B was found to be larger in magnitude when the steel has a higher carbon content.

The connection between DBTT and the cleavage fracture stress can be understood on the basis of a model that was originally suggested by the Russian physicist, Yoffee, in the early 20th century [28]. The Yoffee diagram suggests two generic ways to suppress the ductile-brittle transition: raising the brittle fracture stress (σ_F) or lowering the effective yield strength (σ_y). Since high yield strength is a desirable feature of a structural steel, most of the relevant research has concentrated on raising the brittle fracture stress. The peak tensile stress in the process zone of a crack tip in an elastic–plastic material, σ_T, scales with the yield strength, σ_y, and is of the order of (3–5) σ_y. It follows that this stress increases as the temperature drops. Assuming that the brittle fracture mode is cleavage, then so long as σ_T is below σ_F, the crack tip material yields before cleavage and the fracture is ductile. But in typical ferritic or martensitic steel the thermal increment in σ_y has the consequence that decreasing temperature eventually raises σ_T above σ_F.

When this happens, the material becomes liable to brittle fracture. The ductile–brittle transition occurs at a temperature close to the crossover point.

As illustrated in Figure 7, the most direct way to decrease DBTT is to raise the brittle fracture stress. Grain refinement is an effective way to do this. There are three generic ways to refine the effective grain (block) size of lath martensitic steel:

1. Refine the prior austenite grain size;
2. Break up the block by inserting a second Bain variant;
3. Break up the block by inserting a second phase (usually austenite) along the lath boundaries.

Either thermal or thermomechanical methods allow accomplishing each of these.

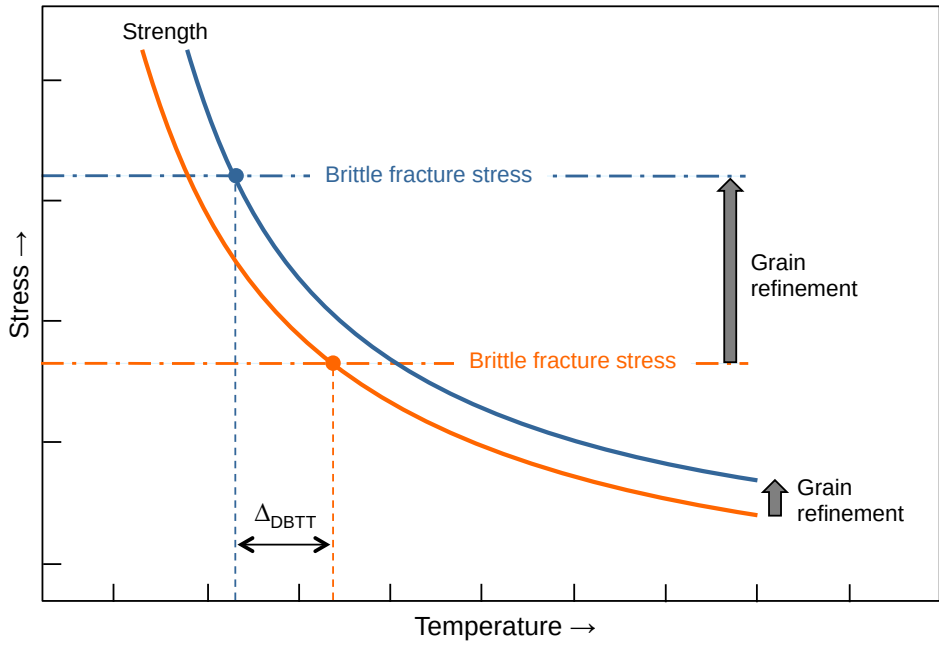

Figure 7. The Yoffee model indicates that ductile–brittle transition occurs when the crack-tip stress exceeds the brittle fracture stress. Refining the grain size raises both stresses, but the effect on fracture stress is generally larger, with the result that DBTT decreases.

Effective Grain Size Against Boundary Embrittlement

Thus far, brittle fracture was associated with transgranular (quasi-) cleavage fracture. However, under certain circumstances, intergranular brittle fracture can be observed. Prior austenite grains usually constitute the facets of that fracture type. The condition for intergranular fracture to occur is the grain boundary cohesion being weaker than the yield strength and cleavage stress.

There are three principal origins for weakening of austenite grain boundaries:

1. Segregation of solutes and impurities to the austenite grain boundary;
2. Precipitation of particles (carbides, nitrides) at the grain boundary;

3. Hydrogen embrittlement.

Refinement of the prior austenite grain size results in an enlarged total grain boundary area. Solute atoms and impurities tend to segregate to the austenite grain boundary. This effect can take place in the austenite phase, ie. before quenching but also after transformation, eg. during a tempering treatment. The increased concentration of interstitials such as carbon, nitrogen, boron in the grain boundary area also leads to a preferred precipitation of metal carbides, nitrides or intermetallic compounds due to the locally increased solubility product. On first sight it may seem that an increased total grain boundary area should lead to a "geometrical dilution" of segregated elements. However, Asahi and Ueno [29] pointed out, based on calculations, that the change in concentration of segregated elements in the grain boundary due to grain refinement is expected to be negligibly small. Therefore they also did not observe a change in distribution and size of precipitates upon tempering.

Hydrogen embrittlement appears to be a boundary phenomenon in ferritic or martensitic steels. Ordinarily, the hydrogen-induced fracture separates prior austenite grain boundaries [30-35] occurring by intergranular decohesion at rather low stress intensities. Increasing yield strength enhances the sensitivity for hydrogen embrittlement, because it increases the local hydrogen concentration at the tip of a stressed crack or notch, and also allows the local cohesive stress to be reached. (Higher yield strength allows higher stress without plastic deformation and as a consequence the lattice dilation caused by the larger stress attracts more hydrogen). Transgranular cracking due to hydrogen embrittlement has also been observed. This fracture mode occurs at higher stress intensities than intergranular decohesion and appears to propagate along planes of maximum shear stress [36]. The fracture appearance resembles that of quasi-cleavage.

Both fracture modes have recently been observed in steel grade 22MnB5 (10B22) in the as-quenched state [37]. The standard 22MnB5 steel comprising an average PAGS of 17 µm had a yield strength of around 1050 MPa and a tensile strength of around 1750 MPa. Charging that steel with hydrogen under a constant applied load led to failure by intergranular fracture at stresses in the range of 400 to 600 MPa, Figure 8. The same steel was then additionally microalloyed with niobium (0.05%), reducing the average PAGS to 6 µm. The strength was marginally increased (+50 MPa) due to this grain refinement. After hydrogen charging, the grain-refined steel showed transgranular cracking with a quasi-cleavage appearance in the fracture initiation area, Figure 9. The fracture stress for this steel was in the range of 1150 to 1250 MPa, ie. above the as-quenched yield strength. Large parts of the fracture surface even showed a ductile dimple-type appearance.

Krauss and co-workers [38] did similar hydrogen embrittlement tests on 10B22 steel and found almost exactly the same drop in fracture stress down to 400 MPa after hydrogen charging, with the appearance of intergranular cracking. Instead of grain refinement, they performed tempering treatments. By low-temperature tempering (150 °C) the same effects in terms of fracture stress and appearance were obtained as in grain-refined 22MnB5.

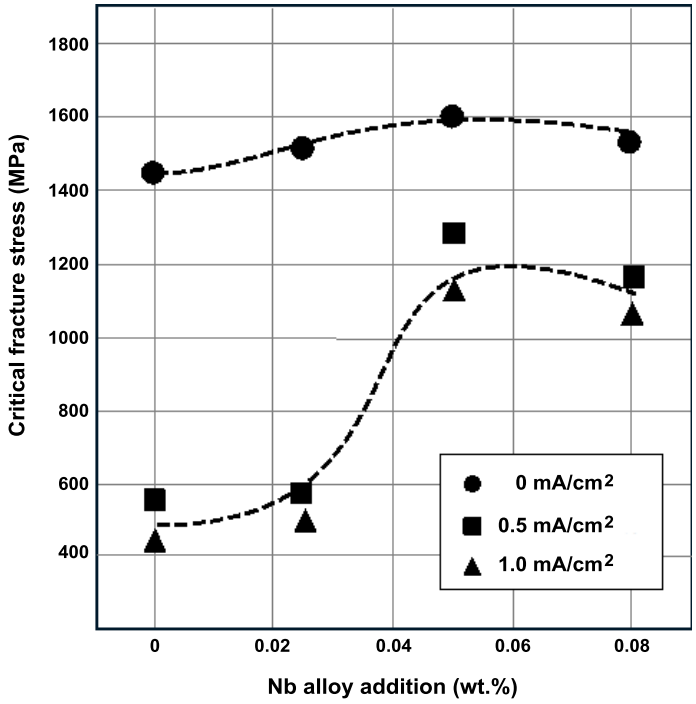

Figure 8. Effect of niobium microalloying on the fracture stress of as-quenched steel 22MnB5 subjected to various conditions of hydrogen charging.

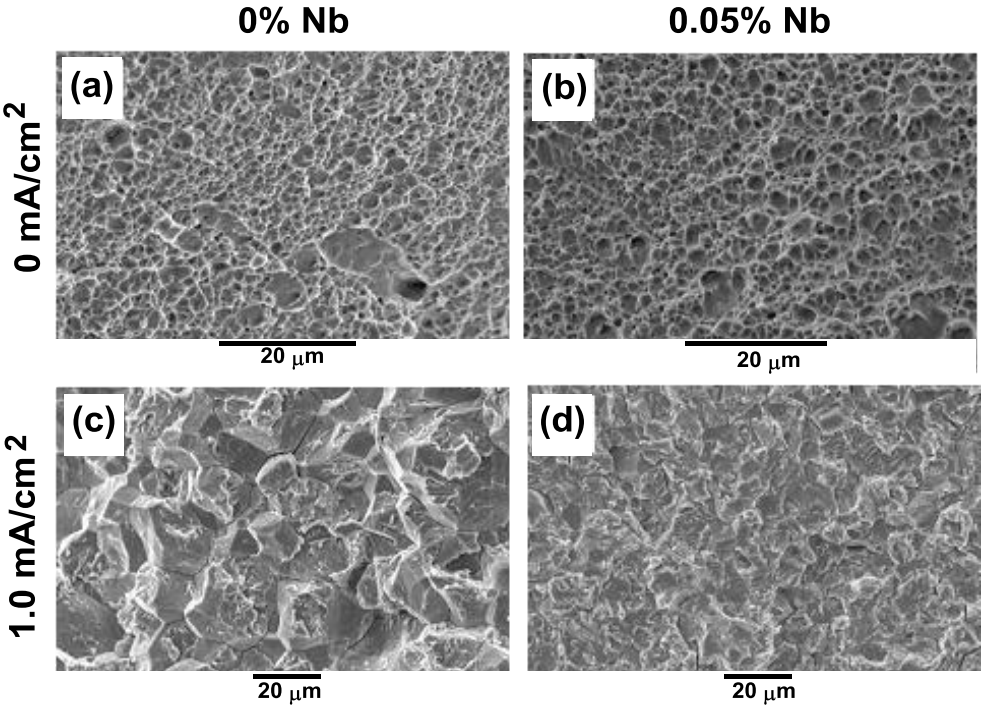

Figure 9. Appearance of fracture surfaces; (a), (b) dimple-type ductile fracture, (c) intergranular brittle fracture, (d) transgranular quasi-cleavage fracture.

In clean or gettered lath martensitic steels, the hydrogen resistance is relatively good and the fracture mode is transgranular [32]. A closer examination shows, however, that even in this case the fracture is primarily interfacial, propagating along martensite lath boundaries. If the fracture is along grain or lath boundaries, then the effective grain size is the length of the semi-planar boundary segments. In lath martensitic steels the boundaries extend across the packet, so the effective grain size is the packet size. To overcome hydrogen embrittlement, it is necessary to refine the packet size to the optimal degree. Rapid reversion treatment ($\alpha' \rightarrow \gamma \rightarrow \alpha'$) produces a coherent product with a submicron packet size, which can make the steel virtually immune to hydrogen embrittlement [28,31].

Effects of Low-temperature Tempering (LTT)

Low-temperature tempering (LTT) improves toughness of as-quenched martensite, but maintains hardness and strength at high levels. In as-quenched martensite the strength originates from carbon atoms trapped in octahedral lattice sites or segregated to dislocations and interfaces of the martensitic structure [1].

When as-quenched martensite is tempered in the temperature range of 150 to 200 °C, transition carbides precipitate in the martensite crystals and retained austenite is stable, Figure 10. Tempering at temperatures above the LTT range causes the transformation of retained austenite and the replacement of the transition carbides by coarser particles of cementite, leading to lower strengths and tempered martensite embrittlement. Krauss [39] explained that the key strengthening mechanism of the LTT structures across the entire spectrum of carbon contents is the strain hardening associated with dynamic interactions of dislocations with the fine transition carbide/dislocation substructure of the tempered martensite [40]. With increasing carbon content, the intensity of these interactions increases as the density of the sub-structural features increases and the spacing of the obstacles to dislocation motion decreases. Secondary factors influencing strain hardening are martensite morphology, prior austenitic grain size (through its effect on martensite packet size), and retained austenite content and distribution.

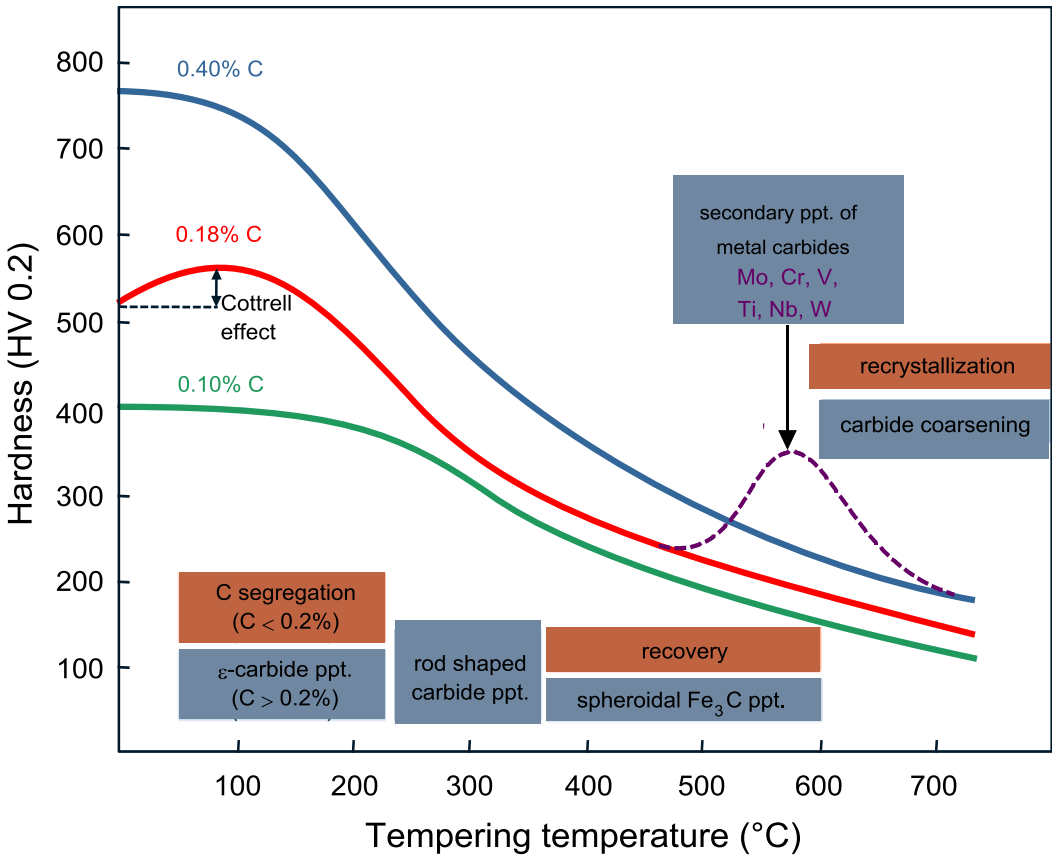

Figure 10. Metallurgical effects occurring during tempering.

Low-carbon martensitic steels are most often produced as plate or sheet and processed into components by cold forming. Therefore, good ductility (in the sense of elongation) is required. As-quenched martensite has high strength but very low total elongation, usually below 10%. LTT brings a small improvement of total elongation at the expense of a moderate loss in tensile strength [41]. The “roundhouse” shape of the stress-strain curve is retained.

Medium-carbon steels are usually hot formed, (eg. by forging, press hardening) so that room temperature elongation is not so important. Such steels require, however, toughness and fracture resistance at ambient and sub-ambient temperatures. Martensitic medium-carbon steels tempered at around 150 °C show significant ability to plastically deform and fail by ductile fracture mechanisms [40]. Engineering stress-strain curves for the low-alloy medium-carbon steels 4130, 4140, and 4150 quenched and tempered at 150 °C show systematic changes in strength and ductility with increasing carbon content. Yield and ultimate tensile strengths of the LTT microstructures increase with carbon content and all measures of ductility, except uniform elongation, decrease with increasing carbon content.

The fracture of all of the LTT martensitic medium-carbon steels occurs by ductile fracture mechanisms, ie. by microvoid nucleation, growth and coalescence, and the macroscopic fracture appearance of the tensile specimens is that of cup-and-cone fracture [40]. Only two components of the LTT martensitic microstructures in medium-carbon steels vary systematically with carbon

content - amount of retained austenite and the density of the transition carbides, which precipitate in the laths of martensite. The more important of these two by far is the transition carbide density. Dislocation movement through the transition carbide/dislocation substructure of the tempered martensitic matrix accomplishes most of the plastic deformation. The higher the transition carbide density, the shorter the dislocation segments which can glide, and the higher the stresses required for dislocation motion and plastic flow. Continuing dynamic interactions between glide dislocations and the transition carbide/dislocation substructure of the tempered martensite during straining, lead to high flow stresses and high rates of strain hardening.

Effects of High-temperature Tempering (HTT)

As-quenched martensitic microstructures are highly unstable during high-temperature tempering [42,43]. The supersaturation of carbon and other elements present in the steel is relieved by precipitation, resulting in dispersions of iron carbides and alloy carbides within the matrix microstructure of the martensite, Figure 10. Retained austenite transforms and produces new distributions of cementite and ferrite.

High-temperature tempering produces remarkable changes in martensitic microstructures. The many types of boundaries change in shape and quantity, changing the shape and size of the crystals, which they enclose. The high density of dislocations produced by the martensitic transformation introduces strain energy into the martensite crystals and drives recovery mechanisms or even recrystallization of tempered martensitic crystal microstructures. In the extreme, microstructures of spheroidized cementite particles and equiaxed ferrite crystals with very low strengths and very high ductilities are produced. However, preceding the formation of such spheroidized microstructures, there are tempering conditions that produce microstructures with excellent combinations of high strength and high fracture resistance. Although the strengths are much reduced from that of as-quenched or low-temperature tempered martensite, the strengths, combined with high toughness, are higher than produced by other processing approaches. Despite the fact that HTT relieves the supersaturation of as-quenched microstructures and produces combinations of ferrite and dispersed carbide particles, high-temperature tempered microstructures still merit the term tempered martensite because martensite is the origin of the structure and traces of the parallel crystal, packet, and block morphology of lath martensite are retained.

The changes produced by high-temperature tempering are continuous as a function of increasing time and temperature of heating and dependent on alloying. Changes that affect performance are the degree to which the dislocation substructure is retained and modified, the elimination, growth, and stabilization of as-quenched martensite crystals (the effective grain size), and the formation of carbide particle dispersions.

Figure 11 shows a light optical micrograph of highly tempered lath martensite in Fe-0.2%C steel [44]. The martensitic microstructure has undergone considerable coarsening, but some parallel boundary alignment of lath martensite is retained. Coarsening of the structure has occurred by the elimination of many of the very fine martensite crystals produced by the martensitic transformation. It appears that the only residual feature of the as-quenched martensite is a block structure in which there are no individual crystals within the blocks. Consistent with current

understanding of lath martensite microstructures in low-carbon steels, the elimination of low angle boundaries probably occurred in blocks of the as-quenched martensite. In addition to the ferritic matrix, dispersed carbide particles (appearing as small dark features) are also part of the HTT microstructure.

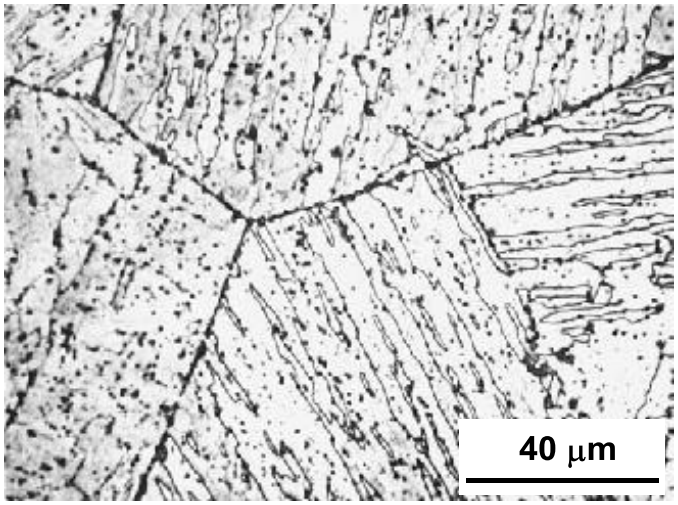

Figure 11. Microstructure of lath martensite in Fe-0.2%C steel after tempering at 700 °C for two hours (light optical micrograph, Nital etch) [44].

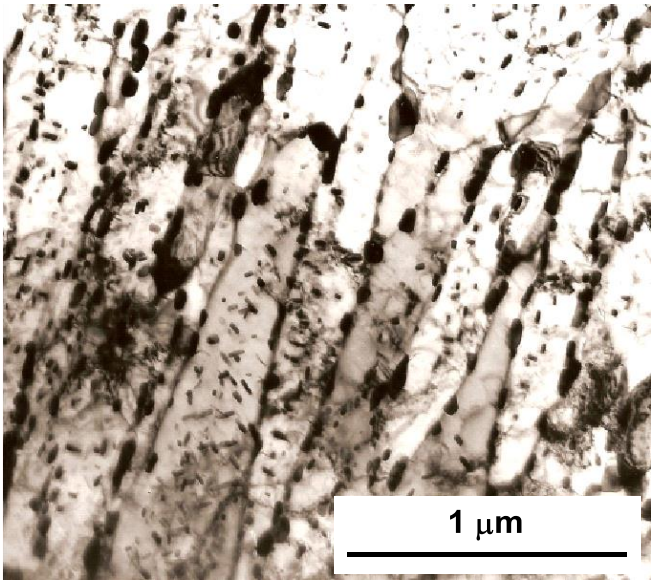

Figure 12. Tempered martensite in 4130 steel heated at 650 °C for one hour (TEM micrograph. Courtesy of F. Woldow while at the Colorado School of Mines).

Not only does the martensite crystal morphology alter during HTT, but the substructure within the martensitic crystals also changes, and as noted relative to Figure 11, carbide particles nucleate and grow. Figure 12 shows a high-magnification TEM micrograph of the microstructure of martensite in a 4130 steel tempered at 650 °C for one hour. Elongated sections of martensite crystals are still parallel. Dispersed carbide particles have formed within martensite crystals and on martensite crystal boundaries and the high dislocation density present within as-quenched martensite has been substantially reduced.

Strengthening would, therefore, come from the very fine grain size, ie. the surviving martensite crystals and perhaps some dispersion strengthening from the carbide particles. The combination of high strength and high toughness of many HTT steels is consistent with the fundamental principle established for ferritic microstructures: grain size refinement is the only strengthening mechanism that increases both strength and toughness [45]. Thus, despite the fact that there is a degree of coarsening of the as-quenched size of the martensite crystals during HTT, the residual very fine crystals or grains account for a major strengthening mechanism in highly tempered martensite. The mechanism and degree of crystal growth, especially in alloy steels, need further research.

Practical applications requiring moderate strength and high toughness are often manufactured from HTT steel. The ductile-to-brittle transition occurs at much lower temperatures than that of microalloyed medium-carbon steels with precipitation-strengthened ferrite/pearlite microstructures treated to comparable hardness. Steels that require good resistance to hydrogen embrittlement are also highly tempered to lower hardness, a property related to the reduction of dislocation density in HTT martensitic steels [29,46-48]. The precipitation of nano-sized alloy carbides in the temperature range of 500 to 650 °C induces a secondary hardening effect. The magnitude of that effect depends on the actual size distribution, as well as type of carbides and can at least compensate in part for the microstructural softening.

Temper Embrittlement

The optimization of strength and toughness by tempering is impeded by the phenomenon of temper embrittlement appearing in the temperature range of 250 to 400 °C and featuring predominantly intergranular cracking along the prior austenite grain boundaries [1]. The embrittlement is concurrent with the replacement of ε-carbide by interlath cementite during tempering and the mechanical instability of interlath films of austenite (as a consequence of carbide precipitation) during subsequent loading, but only occurs in the presence of impurities [49]. Addition of a sufficient amount of silicon to the steel can inhibit the formation of cementite in the critical temperature range. The combination of cementite precipitates and residual impurity elements on prior austenite grain boundaries leads to fracture by intergranular cracking in the embrittlement range.

In the current context, the question arises whether grain refinement would have an effect on temper embrittlement. It has been established that the susceptibility to reverse temper embrittlement (RTE) of tempered martensitic microstructures increases with increasing grain size [50]. This effect can be explained in terms of the ease of brittle crack propagation. In clean, (ie. impurity-free) alloyed steel, the DBTT appears to be insensitive to grain size, in contrast to

plain carbon steels. Substructural features, rather than prior austenite grain size, determine the stress required for brittle cleavage crack propagation in the quenched and tempered alloy steel. When impurities, (eg. Sn, P) are present in the steel, a significant shift of the DBTT towards higher temperatures can be observed, Figure 13. This is accompanied by a change in brittle fracture mode to intergranular, Figure 14. When the grain boundary cohesion is reduced to below the cleavage stress as a consequence of segregated impurities, it equals the yield strength at higher temperature. As expected, intergranular crack propagation is promoted as grain size increases, although segregation occurs at all high-angle grain boundaries. Countermeasures to this effect are to getter solute impurity atoms preventing them from segregating to the grain boundaries. On the other hand, segregation of transition metal atoms can increase the boundary cohesion and counteract intergranular fracture. This effect will be explained in more detail in a later section.

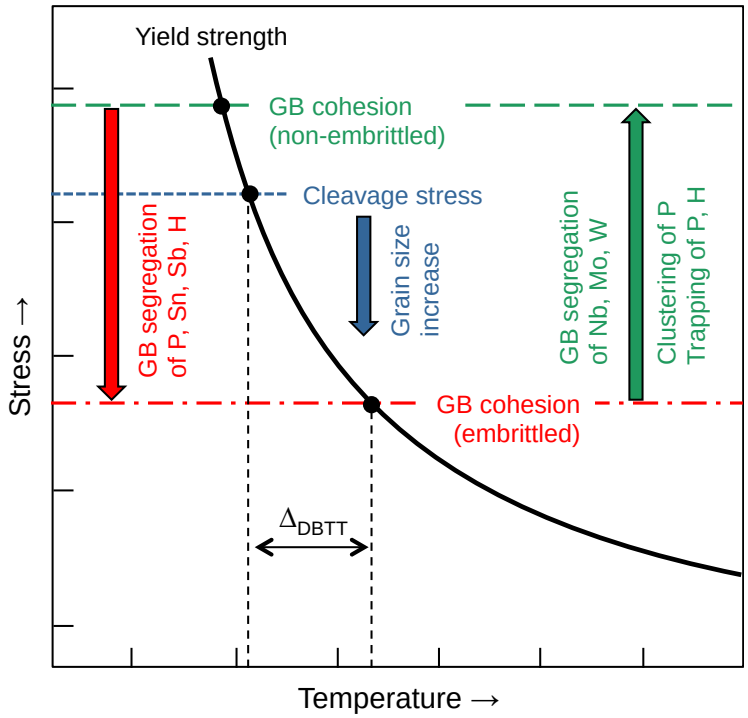

Figure 13. Effect of temperature on the appearance of brittle fracture, influence of boundary embrittlement and metallurgical remedies.

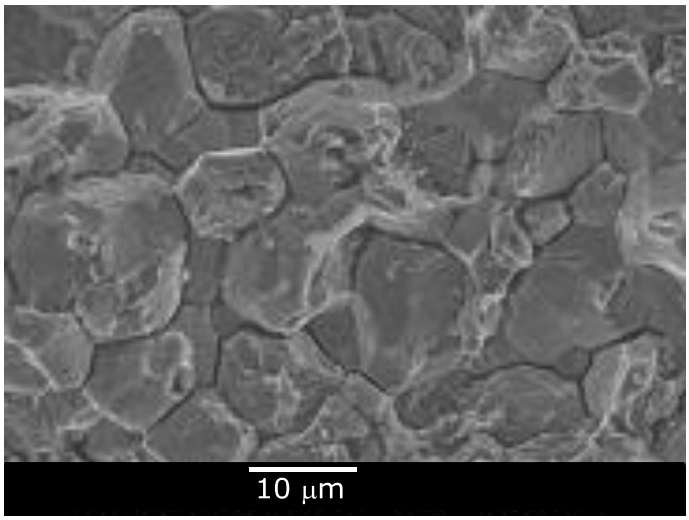

Figure 14. Appearance of intergranular fracture of an embrittled martensitic steel.

As outlined before, the grain size effect on segregated impurity concentration on the boundary is negligible. On the other hand, diffusion distances to boundaries are a direct function of grain size and thus an effect on segregation kinetics should be expected.

Alloy Design and Related Effects

General Considerations

Conventional martensitic steels are usually quenched carbon-manganese grades, often microalloyed with a small amount of boron. In such steel, hardness is determined directly by the carbon content [51]. However, with increasing hardness the toughness of the quench hardened steel decreases to very low values. Alloyed steel types are applied where toughness matters and where through-hardening at heavier gages is required. Guaranteed minimum toughness, (eg. 21 J or 27 J) can be adjusted at low temperature, (eg. 0 °C or -40 °C) by controlling the carbon content and the alloying concept, in combination with appropriate heat treatment. Such grades produce an enhanced service lifetime in applications where impact loads prevail, especially in cold climates.

Alloy Design for Hardenability

A fundamental aspect in designing the alloy for a martensitic steel is hardenability. The alloy design, in combination with the quenching method, must achieve sufficient hardness (strength) over the entire specified depth or thickness of the component. In conventional carbon-manganese steel, the hardening depth is limited to a few millimeters. However, for specific applications, much heavier gages of hardened material are required. Thus, a precisely tuned amount of alloying elements, in combination with high cooling rates, is needed to achieve a high hardness value in the core of thicker plates or components and to obtain a homogeneous microstructure. Even though surface hardness is easily achieved by a quenching or carburizing treatment, hardness tends to decline towards the core of a heavy gage component, with the cooling rate decreasing with distance from the quenched surface. Therefore, hardenability needs to be

enhanced by other alloying elements, such as molybdenum, chromium, copper and nickel. In estimating hardenability by Grange's technique [52] it is assumed that the hardenable diameter for iron is zero. The influence of single alloying elements on the change of the hardenable diameter can be estimated from Figure 15. Besides carbon, molybdenum has the strongest effect before manganese and chromium. Accordingly, adding 0.25%Mo to a Fe-0.2%C base alloy would increase the hardenable cylinder diameter with 90% martensite at the center, by approximately 4 mm.

For a first judgment of the achievable hardening depth, the classic Grossman relationship is often applied [53]. Accordingly, the hardenability of an alloyed steel characterized by the critical diameter *DI* can be calculated based on the critical diameter of the iron-carbon base composition (*DIC*) and multiplying factors (*MF*) for each alloyed element. As mentioned before, a smaller austenite grain size reduces the base hardenability.

$$D_I = D_{IC} \times MF_{Si} \times MF_{Mn} \times MF_{Cr} \times MF_{Mo} \times MF_{Ni} \times MF_V \times MF_{Cu} \times MF_B \times 25.4 \text{ (mm)} \quad (4)$$

$$D_{IC} = (C/10)^{1/2} \times (1.70 - 0.09n) \qquad \text{(in)} \quad (5)$$

C: carbon content in weight percent and *n*: austenite ASTM grain size number.

The use of this method is described in ASTM standard A255-02.

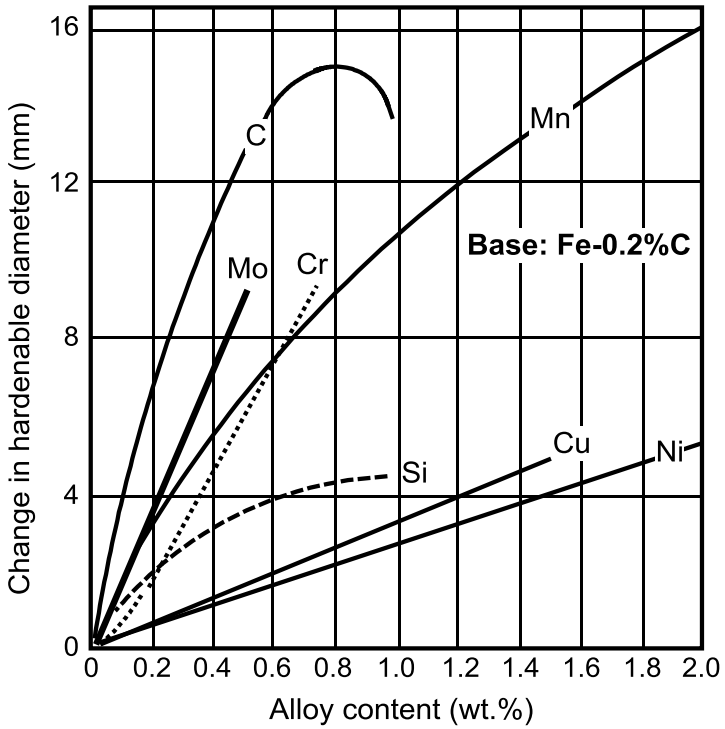

Figure 15. Influence of single alloying elements on the change of the hardenable diameter using Grange's technique.

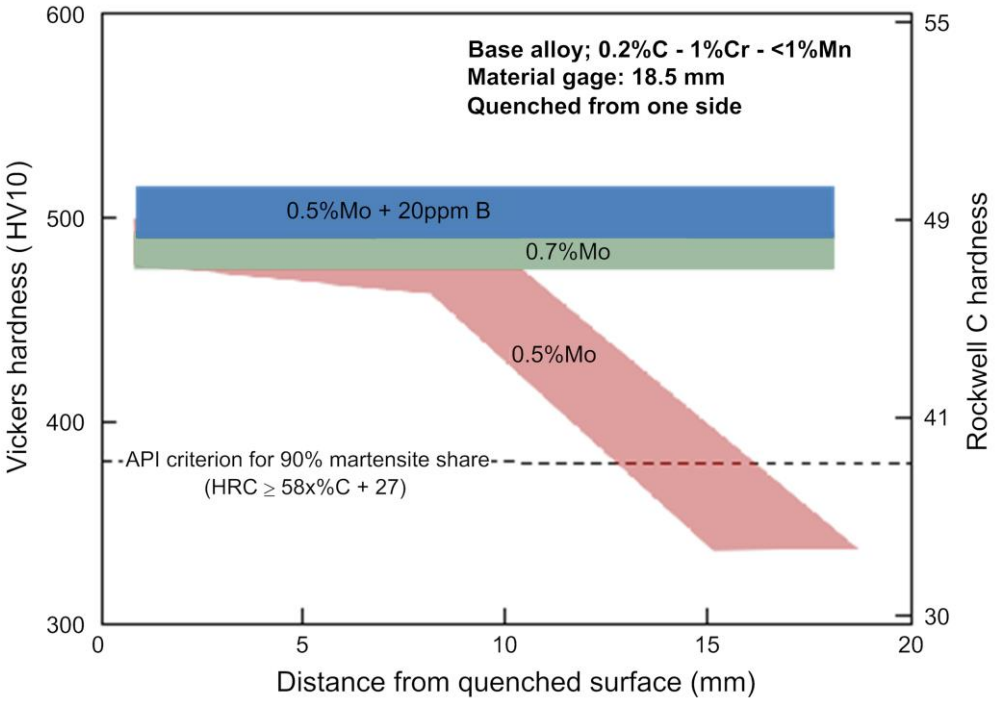

Figure 16. Through-hardenability as a function of Mo and Mo-B dual alloying.

The addition of boron is an efficient method of increasing through-hardenability [54], Figure 16. The specific hardenability effect of boron is to obstruct ferrite nucleation at the austenite grain boundaries. This effect is different from that of manganese, chromium or molybdenum, which lowers the activity of carbon in austenite. To have its effect, solute boron needs to segregate to the austenite grain boundaries before quenching. To keep boron in solid solution, boron nitride formation in austenite needs to be suppressed. This is achieved by adding titanium, which is a much stronger nitride former than boron. Inevitably, TiN particles are formed which have a negative effect on toughness. The grain boundary segregation tendency of boron increases with lowering the austenite temperature. Since carbon also segregates to the austenite grain boundaries, a high carbon-boron solubility product is reached locally. Simultaneously, the solubility limit decreases with the austenite temperature. Consequently, precipitation of intermetallic $Fe_{23}(C,B)_6$ particles on the grain boundary at lower austenite temperatures is likely [55]. The hardenability effect of boron is then lost. Furthermore, these grain boundary precipitates are brittle and deteriorate toughness and DBTT. When the quenching temperature of austenite is too high, insufficient grain boundary segregation of boron occurs and the hardenability effect is hence insufficient. Some processing routes, for instance press hardening or direct quenching, involve a deformation immediately before quenching. Such deformation introduces dislocations on slip planes and develops deformed boundaries at extremely high strain rates [56]. The deformed boundaries are insufficiently covered with boron and the hardenability effect is lost.

Manganese offers a high hardenability effect. However, the element has a pronounced tendency to segregate during casting. These segregation bands are not removed by reheating. Carbon co-segregates with manganese so that the segregation bands have a much higher hardenability than the neighboring areas. Furthermore, the enhanced carbon and manganese content in the segregation band results in a significantly lower martensite start temperature. The consequence is, firstly, an inhomogeneous hardness distribution in the quenched steel and, secondly, the presence of high residual stresses due to the difference in martensite start temperature. Both effects are detrimental to toughness, Figure 17. Moreover, macroscopic residual stresses lead to distortion, negatively affect fatigue resistance and in the presence of hydrogen, promote delayed cracking.

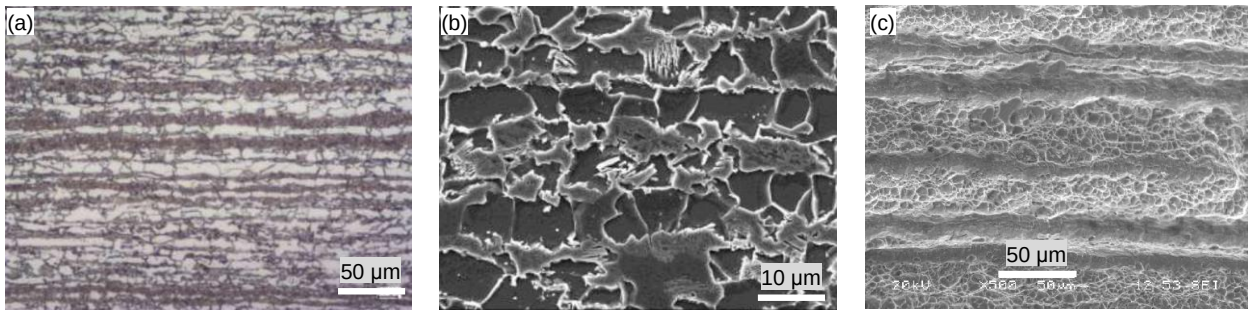

Figure 17. Banded ferritic-pearlitic microstructure of hot rolled 22MnB5 (1.8%Mn) prior to hardening; (a) LOM and (b) SEM. (c) Tensile test at room temperature showing brittle fracture in Mn segregation bands, ductile fracture in softer Mn-depleted areas.

As mentioned before, molybdenum is particularly efficient in providing good hardenability. It does not show the segregation tendency of manganese and its effect on lowering the martensite start temperature is weaker. Molybdenum's hardenability effect is demonstrated in Figure 18 for a steel with a base composition of 0.5%Mn and 0.3%Si at carbon levels ranging from 0.1 to 1.1%. The Grossmann relationship is based on the assumption that there are no interactions between carbon and the alloying elements or between the various alloying elements. However, from Figure 18 it becomes evident that molybdenum's multiplying factor varies with the carbon content [53].

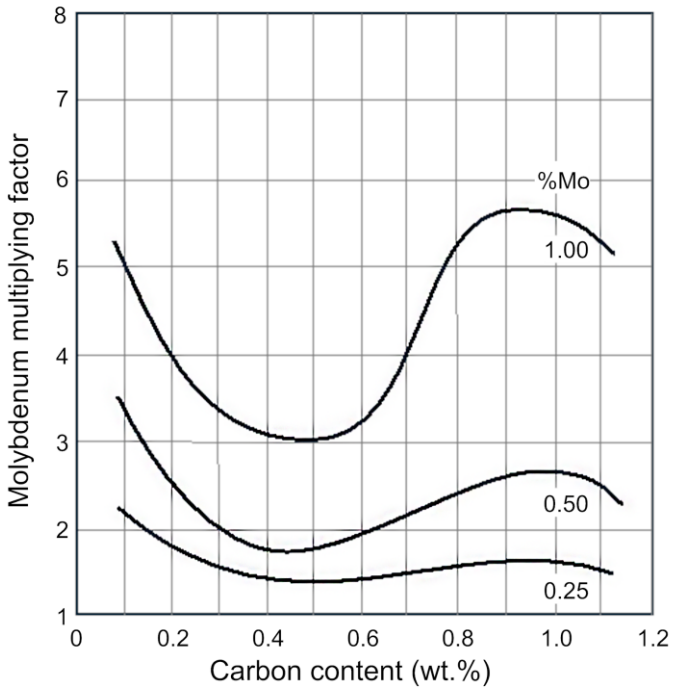

Figure 18. Effect of molybdenum and carbon on the molybdenum multiplying factor of steels containing 0.5%Mn and 0.3%Si.

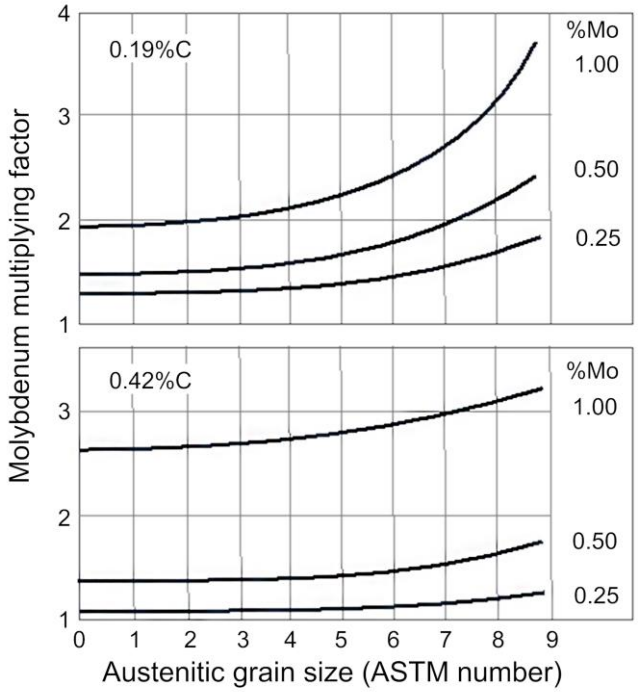

Figure 19. Effect of austenite grain size on the molybdenum multiplying factor of steels containing 0.5%Mn and 0.3%Si.

Especially in the range of low- and medium-carbon steels, the multiplying factor decreases with increasing carbon content reaching a minimum at around 0.45%C. This means that molybdenum is particularly effective in raising the hardenability of such steels with reduced carbon equivalent (CE). The amount of molybdenum needed naturally depends on the hardened gage to be produced. Thicker gages require a larger Mo addition.

Especially at lower carbon levels, the multiplying factor for molybdenum also strongly depends on the PAGS [57]. When the austenite grain size decreases, the multiplying factor increases progressively, Figure 19. Thus, molybdenum alloying can effectively counteract the loss of hardenability caused by grain refinement. This effect is very important since grain refinement of the austenite structure is to be aimed at according to the reasons outlined before.

With regard to further increasing hardenability, the combination of molybdenum with chromium appears to have a strong synergy. The combined effect of these two elements is much stronger than that of manganese and chromium, Figure 20. Accordingly, the production of heavy gaged steel typically relies on combined alloying of molybdenum and chromium. The further addition of nickel is particularly interesting when good low-temperature toughness is desired.

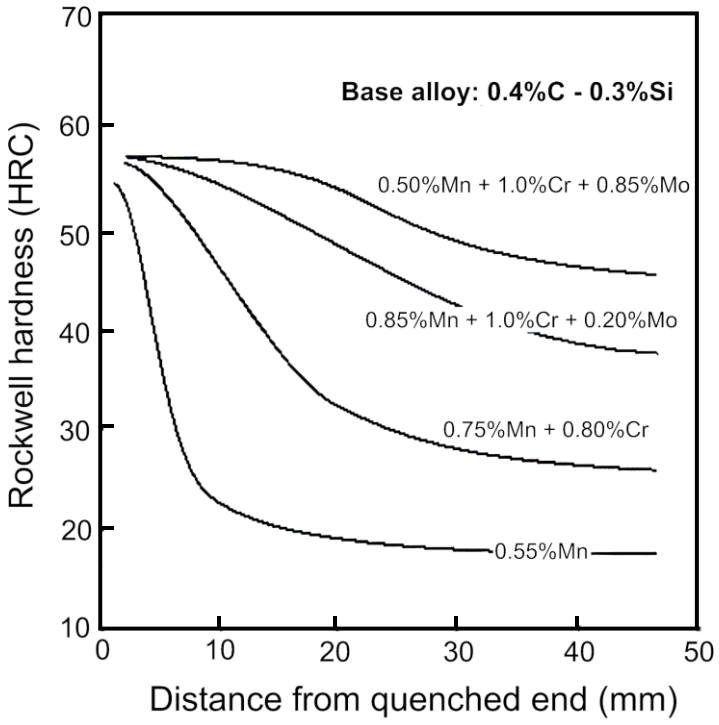

Figure 20. Effect of alloying elements on the Jominy hardenability curves of steels containing 0.4%C and 0.3%Si.

Alloy Design for Grain Refinement

Based on the fundamentals detailed at the start of this paper, it is very evident that grain refinement is the major target in optimizing mechanical properties of martensitic steel. Considering the various processing routes for producing martensitic steel, the following steps have an influence on the PAGS:

- Soaking treatment (>1100 °C) – austenite grain growth;
- Roughing hot deformation – austenite grain homogenization and moderate refinement;
- Finish hot deformation – austenite grain refinement depending on rolling schedule;
- Annealing after cold deformation – recrystallization and ferrite grain growth;
- Reheating before quenching – austenite grain coarsening;
- Case carburizing treatment – austenite grain coarsening.

Any grain refining action starts from the grain size distribution present in the hot steel at the end of the soaking treatment. Depending on temperature and duration of soaking, the austenite grains can become rather large in size. A successful way of limiting the austenite grain growth during soaking is the dispersion of fine TiN particles. TiN has very high-temperature stability, Figure 21, and can thus pin austenite grain boundaries. In order to have this pinning effect maximized, it is advisable to adjust the titanium addition to a near-stoichiometric ratio with the residual nitrogen in the steel (nitrogen is in the range of 30 to 100 ppm depending on the steelmaking process). Considering the stoichiometric ratio of 3.4, the optimum titanium addition is in the range of 100 to 350 ppm. Over-stoichiometric addition of titanium leads to precipitation of coarse TiN particles in the liquid steel, Figure 21. The presence of such particles is harmful to toughness. This guideline should also be observed when adding titanium for protecting boron against nitrogen.

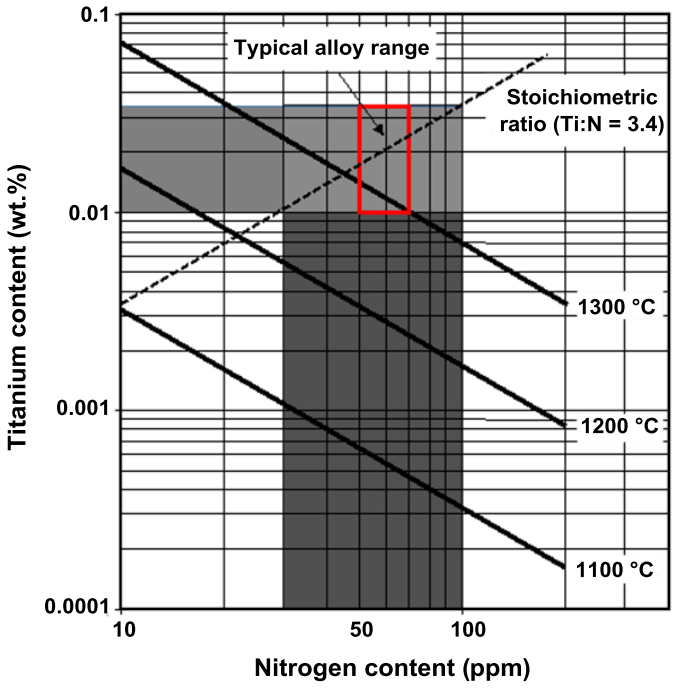

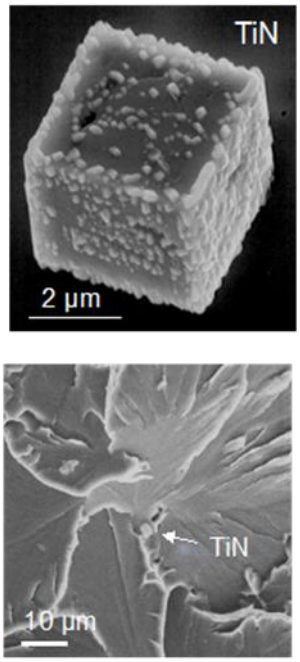

Figure 21. Solubility isotherms for titanium nitride and morphology of coarse TiN particle initiating fracture in a Charpy impact test.

Roughing hot deformation should be done at temperatures above the recrystallization limit temperature (RLT) to allow a thorough homogenization of the microstructure. Multiple deformation passes with subsequent recrystallization can achieve moderate grain refinement. The addition of recrystallization delaying elements, such as niobium and molybdenum has to be matched to the temperature window available for roughing.

Finishing hot deformation below the recrystallization-stop temperature (FRT<RST) allows achievement of the largest grain size reduction. It is well established that niobium is most effective in retarding the static recrystallization (SRX) of austenite at high temperatures, Figure 22. This effect of niobium strongly increases up to an addition of 0.06% and then levels off [58]. Molybdenum, as a single alloying element, does not remarkably retard SRX. However, the combination of Mo and niobium leads to a synergetic increase in retardation of SRX. Earlier experiments performed by Akben et al., [59], revealed the effect of molybdenum additions on the dynamic recrystallization (DRX) of microalloyed steels. When microalloyed steels are deformed above the solution temperature of their respective carbonitrides, the addition of molybdenum leads to a distinct retardation in the initiation of dynamic recrystallization. The solute retarding effect of molybdenum alone is intermediate between that of niobium, which has the greatest and that of vanadium, which has the least effect, on an equal atom fraction basis. The addition of boron alone can slightly retard SRX. However, when boron is combined with niobium, the effect is larger than the sum of the separate effects. According to He et al., [60], this has been attributed to the formation of Nb-B complexes exerting a strong dragging force on the grain boundaries and hence reducing their mobility. Increasing the recrystallization stop temperature (RST) to values of 900 °C or above results in a particularly large processing window for finish rolling. The increased recrystallization limit temperature (RLT) observed for co-addition of boron can be a

concern, as full recrystallization is desired during roughing. Especially for plate mills, the operating window is narrowed due to the relatively low slab discharge temperature.

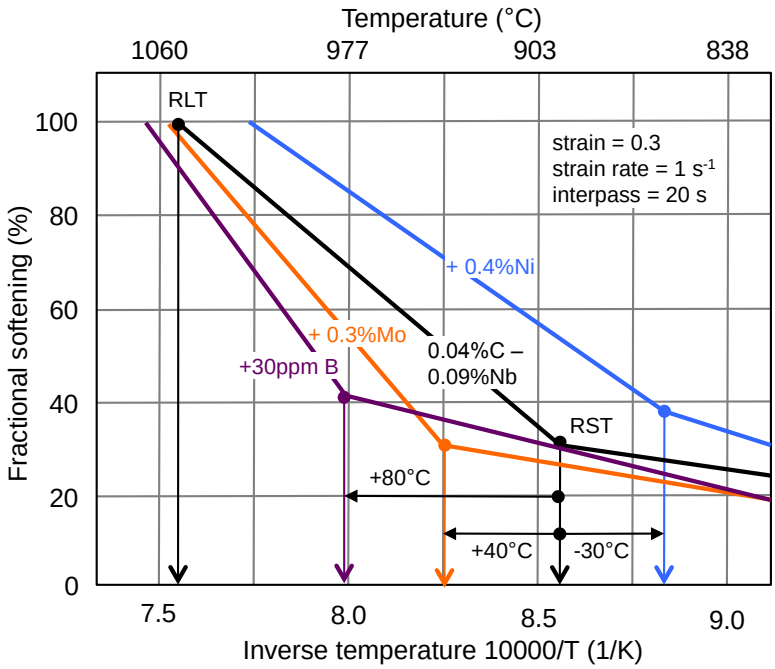

Figure 22. Effect of boron, molybdenum and nickel on the recrystallization behavior in low-carbon, high-niobium steels.

When niobium microalloyed steel is ausformed below the solution temperature of its carbide or carbonitride, in-situ precipitation of small particles results in a further component of retarding recrystallization. In this case, the addition of molybdenum involves two opposing effects. One is an increased retardation of recrystallization due to its effect as a solute. The other is a decrease in the amount of precipitation due to reduced activity of carbon and nitrogen. It was observed that the onset of precipitation of niobium in a 0.05%C-0.04%Nb steel takes twice as long when 0.3%Mo is added [59]. More recent results by Cao [61] confirmed this effect and indicated that the precipitation start in a 0.02%C-0.08%Nb steel is delayed by one order of magnitude after adding 0.15%Mo. It is evident that an increased portion of niobium can be retained in solid solution. Niobium prevailing in solid solution after finish rolling has a significant capability of reducing the transformation temperature. Solute molybdenum and niobium both strongly reduce the diffusivity of carbon in austenite [62]. This effect is stronger for niobium than for molybdenum. However, niobium's solubility is limited and decreases with temperature, whereas molybdenum remains fully soluble. Since molybdenum retards the niobium precipitation as explained above, their individual effects on reducing the carbon activity are additive in dual alloyed steel. Hara et al. [63] have explained the effect of reduced carbon activity by Nb-C or Mo-C cluster formation. Microalloying elements available in solid solution after finish rolling have two important effects. Firstly, they delay the transformation from austenite to ferrite to a lower temperature. This effect increases with the cooling speed. Secondly, solute microalloying elements have the potential to precipitate during or after the phase transformation to a much finer particle size than that of precipitates formed in austenite. Upon direct quenching these precipitates can provide effective secondary hardening during a subsequent tempering treatment.

Alloy Design for Tempering Resistance

In steels alloyed with strong carbide-forming elements, such as chromium and molybdenum, high-temperature tempering permits the diffusion of the alloying elements into the cementite which precipitates and grows in HTT microstructures. It has long been known that those elements significantly reduce the rate at which hardness decreases during high-temperature tempering [51]. Recently, atom probe tomography has made it possible to determine the distribution of elements on an atomic scale. Accordingly, the carbide forming elements are shown to be beginning to diffuse into the cementite of 4340 steel tempered at 575 °C [64]. The study also showed that at a lower tempering temperature of 325 °C cementite forms without any substitutional alloying elements. Thus at the higher temperatures at which substitutional atoms can noticeably diffuse, their partial but still sluggish diffusion restricts cementite particle growth.

Molybdenum mitigates the strength loss during high-temperature tempering in two further ways: through solid solution strengthening, as well as secondary precipitation of complex carbides, together with other elements, such as chromium and niobium. Through its capability of forming such carbides, molybdenum is very efficient in delaying the loss of strength during tempering while improving fracture toughness. Figure 23 demonstrates this effect of molybdenum in combination with chromium and niobium for various Holloman-Parameters (HP) defined as:

$$HP = T\,x\,(20 + log\ t)\,x\,10^{-3} \tag{6}$$

where T is the tempering temperature in Kelvin and t the tempering duration in hours. Increasing molybdenum content clearly improves the tempering resistance of the Mn-Cr steel, however, superior tempering resistance is obtained by a combination of molybdenum and niobium, Figure 23. For a selected HP value, one can either temper at lower temperature for longer time or at higher temperature for a shorter duration. Tempering at high temperatures in the region below the A_{c1}-transformation point brings about the most desirable microstructure in terms of SSC (sulfide stress cracking) resistance. A well-recovered matrix with uniformly dispersed spheroidized carbide particles are the main characteristic of this microstructure.

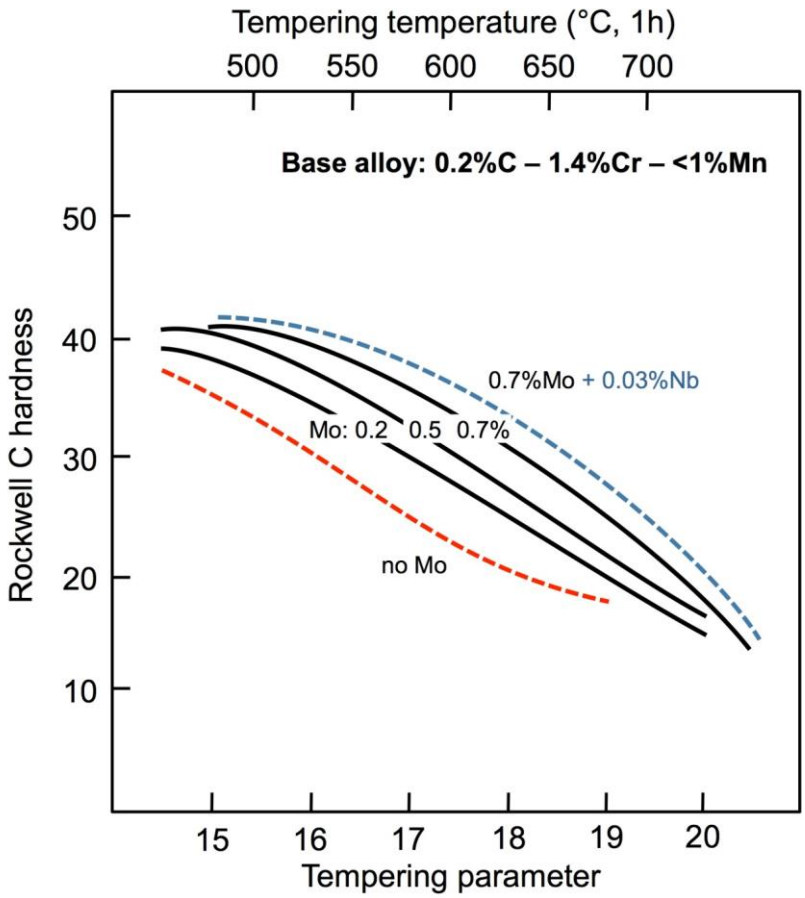

Figure 23. Tempering behavior of quenched steel for various molybdenum additions and niobium microalloying.

As testimony of molybdenum-alloyed steel's good tempering resistance, the martensite in a 0.12%C-steel alloyed with 1.40%Mn and 0.29%Mo was found to contain a reduced but still high dislocation density upon tempering at 675 °C [65]. Figure 24 shows the beginning of recrystallization in this HTT steel, a mechanism that converts the tempered martensite into an equiaxed ferrite/spheroidized microstructure with substantially lower hardness and strength than the tempered martensite it replaces.

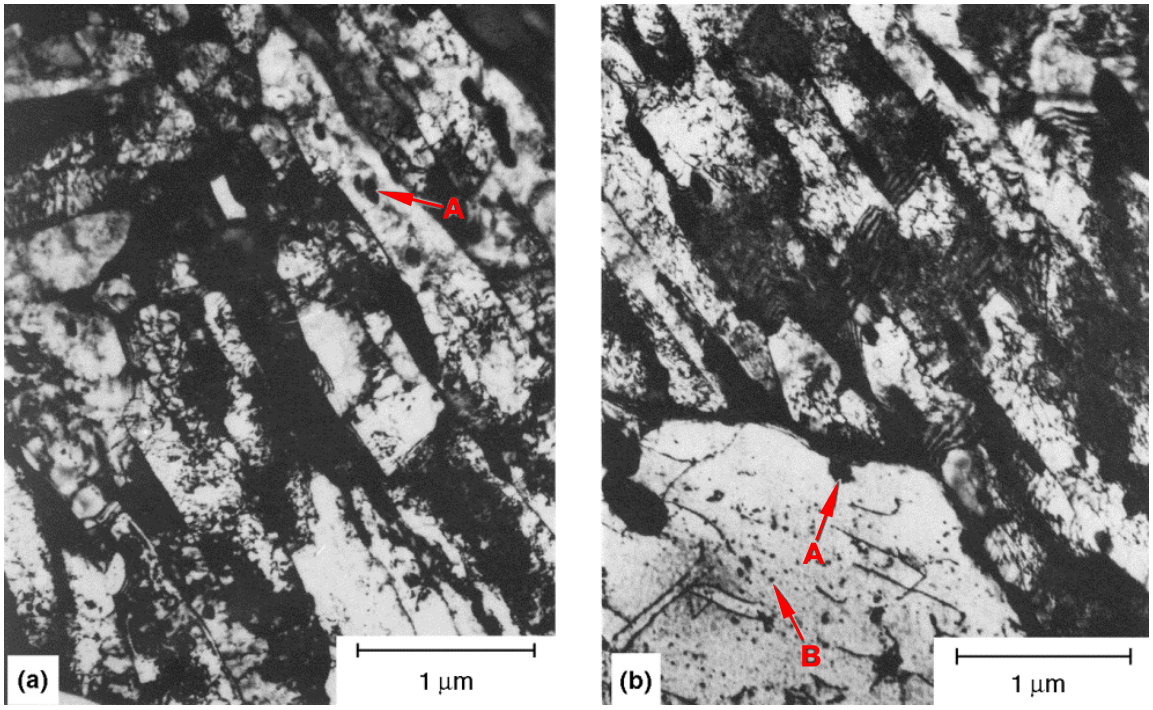

Figure 24. TEM micrographs showing the onset of recrystallization in a 0.12%C steel alloyed with 1.40%Mn and 0.29%Mo; tempered at 675 °C for; (a) one hour and (b) two hours [65]. A and B show larger and smaller spheroidized cementite and carbide particles within recrystallized ferrite grains

Boron microalloyed Cr-Mo steel has a higher tempering resistance than boron-free steel, especially at elevated tempering temperatures. However, boron-treated steel, tempered at higher temperature, has clearly inferior room temperature toughness as compared to the boron-free steel. Particularly when tempering at 600 °C, boron-treated steel tends to have low toughness due to formation of continuous cementite films on the lath boundaries. After tempering above 700 °C, boron-free steels show extensive recovery with the onset of recrystallization resulting in good toughness, whereas in boron-treated steel, recrystallization is retarded so that its toughness is still inferior. A significant problem is the formation of $Fe_{23}(C,B)_6$ precipitates on the prior austenite grain boundaries. This intermetallic phase is brittle and significantly impairs the DBTT. Maitrepierre et al., [66], discussed this phenomenon in detail showing that over-alloying with boron is particularly harmful. The best compromise between hardenability and toughness, after high-temperature tempering, is found for boron additions between 10 and 30 ppm. However, in practice it is a challenge for the melt shop of a steel mill to meet this narrow window.

The carbide reactions in molybdenum steels are extremely slow, and therefore, hard to complete by heat treatment at 700 °C [67]. As a result of this, it is often observed that carbides present in a steel transformed isothermally at 700 °C, differ from those in steel tempered at the same temperature. $M_{23}C_6$ is found in tempered structures of molybdenum-alloyed steels containing chromium as an additional alloying element. In this carbide type, molybdenum substitutes a fraction of the chromium atoms.

Long-time annealing of molybdenum-only alloyed carbon steel results in the formation of needle-shaped Mo_2C precipitates in the grain interior [68], Figure 25. Depending on the C/Mo ratio they can be nearly pure Mo_2C [69]. This is particularly the case when the atomic C/Mo ratio is around stoichiometry. The needles have a preferred orientation and grow along the <100> direction in the ferrite lattice, Figure 25. The average length of Mo_2C needles increases with the annealing duration. These Mo_2C needle shaped precipitates should be avoided, as they are particularly harmful when hydrogen is present in the steel. Lower molybdenum content (≤0.3%) does not cause this problem, Figure 26. For higher molybdenum contents, the addition of stronger carbide formers (microalloys) is advisable.

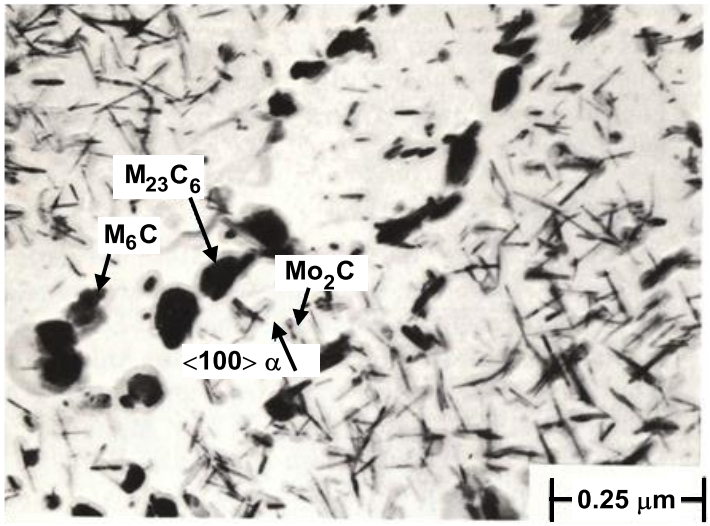

Figure 25. Types of molybdenum-containing precipitates in a 0.2%C-0.5%Mo steel after tempering for 16 h at 700 °C [67].

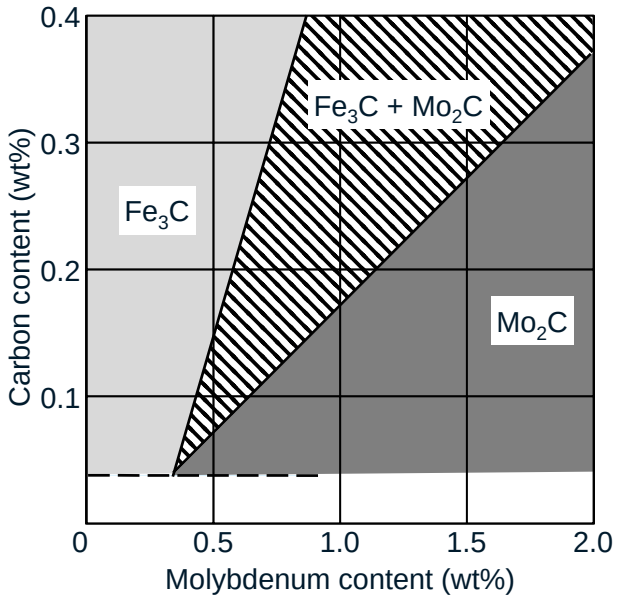

Figure 26. Conditions for Mo_2C precipitate formation during long term annealing at 700 °C.

Several other alloying elements have an influence on strength during high-temperature tempering. The effects of the most typical alloying elements in Q&T steels have been determined by a range of experiments and subsequent multiple regression analysis. The strength correlations for a given quench and temper condition are shown in Table I [70].

According to the formulae in Table I, manganese alloying leads to a yield strength reduction, whereas molybdenum raises yield and tensile strength. Thus, molybdenum not only provides a better hardenability than manganese but also boosts secondary hardening during tempering.

Table I. Effect of Alloying Elements in wt.% on Strength after Q&T Treatment
(930 °C/30 min. → oil-quench → 600 °C/60 min. → air-cool)

Yield strength = (MPa)	$715 + 1880\,[C]^2 - 1663\,[C]^3 + 67\,[Si] - 774\,[Mn] + 920\,[Mn]^2 - 330\,[Mn]^3 + 74\,[Cr] - 16\,[Cr]^3 - 3.5\,[Ni]^2 + 453\,[Mo] - 181\,[Mo]^2 + 124\,[W]^2 + 1820\,[V] - 5226\,[V]^2 + 4957\,[V]^3 + 425\,[Nb] + 22114\,[Al]^2 + 12550\,[N] - 972x10^4\,[N]^3$
Tensile strength = (MPa)	$534 + 865\,[C] + 162\,[Si] - 62\,[Si]^2 + 3\,[Ni]^2 + 579\,[Mo] - 252\,[Mo]^2 + 291\,[W] - 368\,[W]^2 + 1389\,[V] - 2305\,[V]^2 - 252\,[Ti] + 10635\,[N] - 783x10^4\,[N]^3$

Alloy Design Against Temper Embrittlement

Impurity elements such as phosphorus, antimony and tin are notorious for their embrittling effect. Therefore, the content of these elements must be limited as much as possible during steelmaking. Phosphorous is one of the most frequent impurities in steels. It can affect material properties strongly, even at small bulk concentrations of 100 ppm if it is segregated at the grain boundaries. In simple carbon steels the tendency for grain boundary segregation of phosphorus is reduced due to site competition at the grain boundary [71]. In alloy steel, however, a significant portion of carbon becomes tied up as metal carbide during high-temperature tempering and phosphorus grain boundary segregation can occur. The problem also appears in high strength interstitial-free (IF) steels for automotive applications. These steels, which are phosphorus alloyed and where carbon is completely tied up, are vulnerable to secondary work embrittlement. The traditional remedy against embrittlement is the addition of 5-10 ppm boron, Figure 27. Site competition by solute boron can successfully avoid grain boundary segregation of phosphorus during annealing treatments [72,73]. Later it was demonstrated by Urabe et al., [74], that boron-free high strength IF steel with an over-stoichiometric niobium addition produces a similar resistance against embrittlement. Two different metallurgical reasons can explain the anti-embrittlement effect of niobium. In carbon-free steel (such as IF steel) niobium has been shown to form NbP clusters or even precipitates [75]. This effect disappears when solute carbon is present leading to NbC precipitation. Likewise, titanium forms TiP clusters in carbon-free steel, reducing embrittlement. When solute niobium and titanium are segregated to the grain boundary they appear to increase boundary cohesion. Starting from first-principles quantum mechanical calculations on the strengthening and embrittling effects of alloying metals on the grain boundary cohesion, it was found that many transition metals of the groups IVa to VIIa have the potency of increasing cohesion, Figure 28 [76]. Of those technically relevant in steelmaking, tungsten, niobium and molybdenum have the largest effects in descending order. Titanium and vanadium have a clearly smaller cohesion enhancing effect, whereas manganese has a cohesion reducing effect, thus supporting embrittlement.

Both molybdenum and tungsten have rather good solubility in medium carbon steel [77], contrary to niobium and accordingly these are most suitable to deploy the cohesion enhancing effect, especially in medium-carbon and high-carbon steels. Again it appears that higher manganese additions should be avoided.

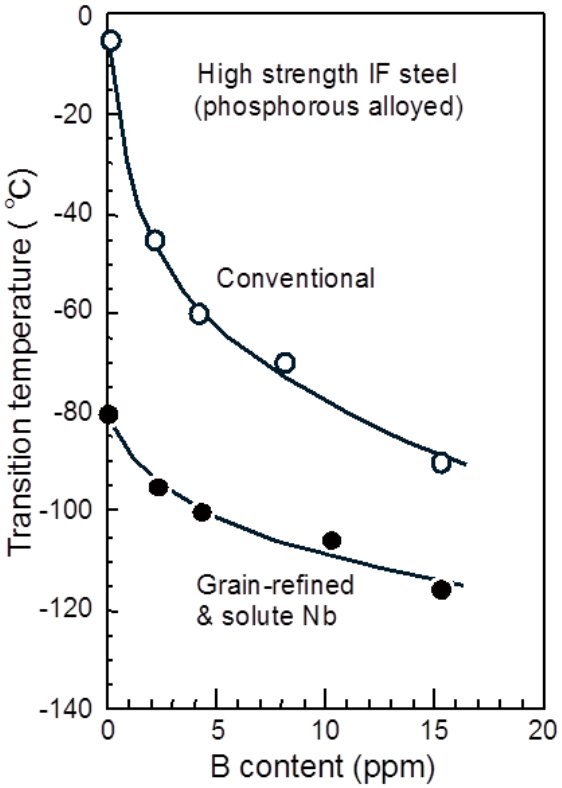

Figure 27. Avoidance of phosphorus grain boundary embrittlement by boron and solute niobium [74].

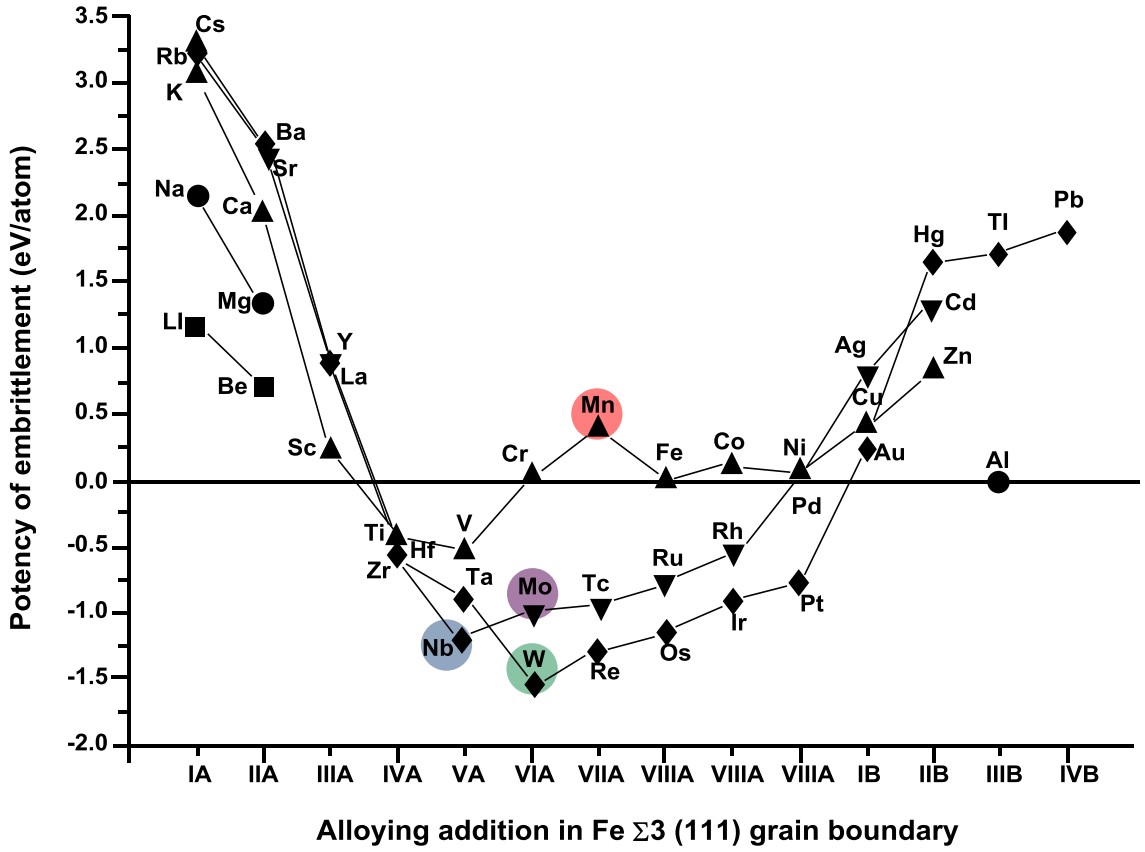

Figure 28. Embrittlement potency of substitutional additions in Fe Σ3(111) grain boundary [76].

Alloy Design Against Hydrogen Embrittlement

Hydrogen embrittlement is a severe concern in practically all ultra-high strength steels. The principal effect of hydrogen embrittlement has been already discussed in this paper where grain refinement was identified as a feasible means of reducing this detrimental effect. Another means of reducing hydrogen embrittlement is that of hydrogen trapping.

The concept of hydrogen trapping, Figure 29, has significant potential with regard to reducing the sensitivity of steel to hydrogen induced delayed cracking. Various traps are characterized by their binding energy of hydrogen, Table II [78-81]. Flat traps with binding energies of <20 kJ/mol can be discerned from deep traps with binding energies of >50 kJ/mol [79]. Grain boundaries, coherent precipitates, and dislocations form a class of reversible traps, which can only weakly bind hydrogen at temperatures of interest. Incoherent precipitates, voids, etc. are much stronger irreversible traps. It is the latter type of trap that appears most effective in modifying susceptibility to delayed cracking in the presence of hydrogen. Both improvement and degradation are possible depending on the shape, location and specific properties of irreversible traps. However, reversible (weak) traps can also play an important role since they may strongly affect the kinetics of hydrogen transport. In particular, their presence can often reduce susceptibility by increasing the time necessary to reach some critical local hydrogen concentration [78]. Important exceptions are mobile dislocations, which transport hydrogen in

their core or as Cottrell-type atmospheres. These mobile traps can transport hydrogen at a much faster rate than by lattice diffusion and with a specificity of location that provides an efficient means of rapidly localizing the hydrogen concentration at strong microstructural traps [82]. If these are local failure centers, embrittlement can be enhanced. There is evidence for the occurrence of this scenario in a number of alloy systems [83-87].

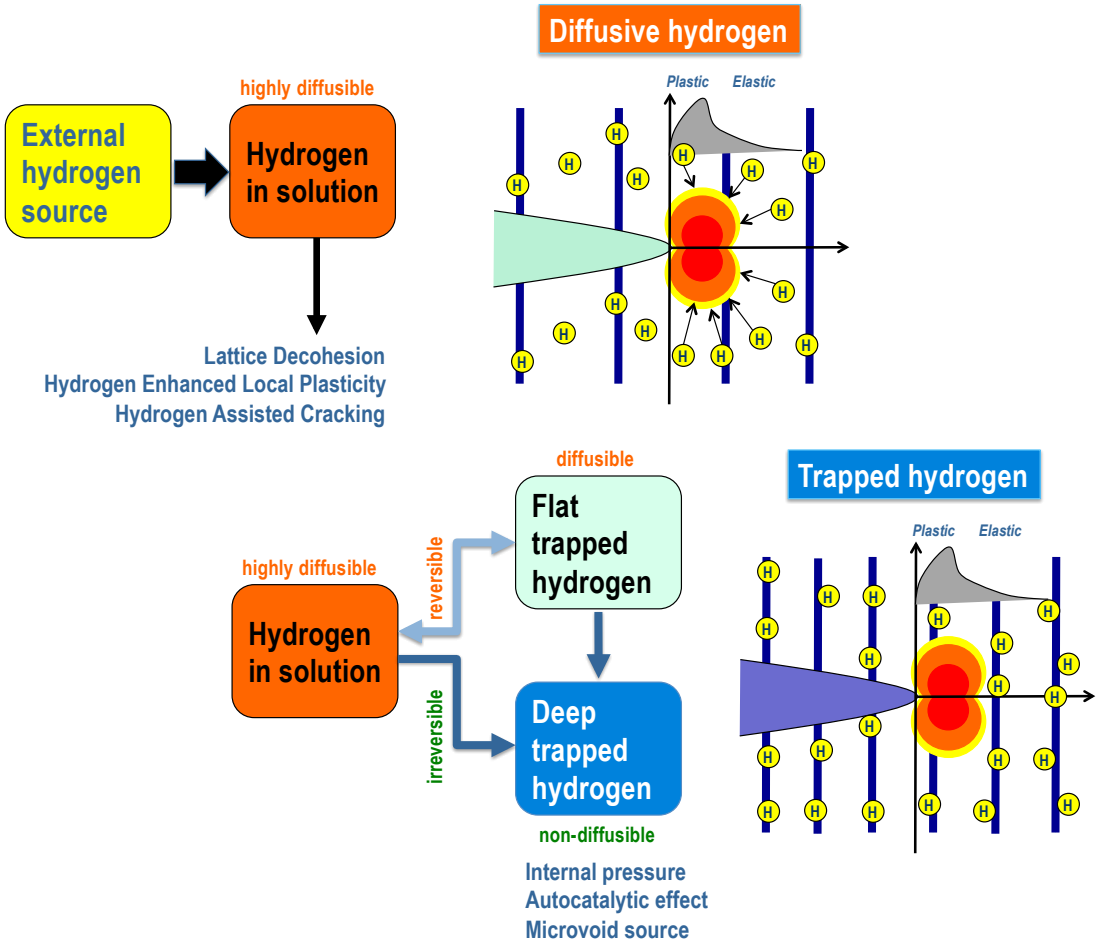

Figure 29. Effects of diffusible hydrogen and concept of hydrogen trapping.

Table II. Hydrogen Trapping Energy of Various Nitrides and Carbides in an Iron Matrix [79]

Alloy system	**Fe-Zr-N**	**Fe-Ti-N**	**Fe-Nb-N**	**Fe-V-N**	**Fe-Mo-N**
Flat traps (kJ/mol H)	-20.4	-20.7	-18.2	-18.9	-19.3
Deep traps (kJ/mol H)	-56.1	-60.5	-54.9	-56.0	-56.0
Alloy system	**Fe-Zr-C**	**Fe-Ti-C**	**Fe-Nb-C**	**Fe-V-C**	**Fe-Mo-C**
Flat traps (kJ/mol H)	-19.9	-20.6	-18.3	-17.2	-13.9
Deep traps (kJ/mol H)	-58.5	-58.5	-56.0	-57.0	-56.5

Numerous studies have confirmed the hydrogen trapping performance of microalloy precipitates. Asahi et al., [88], identified vanadium carbide as a hydrogen trap site in a steel with a tempered martensite structure. The activation energy for de-trapping is in the order of 30 kJ/mol. The de-trapping of hydrogen is very slow while the trapping presumably proceeds rapidly. Similar experiments by Yokota and Shiraga [89] showed that the tempering condition is very important to optimize the trapping effect of vanadium carbide. Wei et al., [90], demonstrated the trapping capability of TiC in a quenched and tempered steel of 0.42%C. TiC is present in a bimodal size distribution. Fine TiC particles were found to be more effective in trapping hydrogen than coarse particles with the same volume fraction.

In high strength seamless tubes, the distribution of spheroid shaped carbide precipitates was shown to allow a significantly higher critical stress level under hydrogen loaded conditions [91,92]. In such medium carbon (0.25-0.45%) steels, niobium has been microalloyed up to 0.08%, providing a fine-grained microstructure and a homogeneous distribution of precipitates. Additions of vanadium in combination with a suitable tempering treatment further increase the performance under hydrogen-loaded conditions by creating additional trapping sites.

In spring steels, vanadium and titanium precipitates were shown to trap hydrogen and thus to improve corrosion fatigue properties. It appeared that titanium precipitates had a bigger effect than those of vanadium [93]. A suspension spring steel designed for 1200 MPa shear stress by Daido Steel [94] makes use of boron and niobium microalloying to increase the delayed fracture strength. Simultaneously, the corrosion-fatigue resistance is also significantly improved. Perrard et al., [95], identified a microalloying combination of niobium and titanium as the most effective solution, particularly with respect to corrosion-fatigue endurance, when developing ultra-high strength spring steel.

When designing the alloy concept for hydrogen trapping by precipitates, the intended processing route needs to be considered with respect to the precipitation behavior of the various transition metal carbides. When producing as-quenched or low-temperature tempered martensite, vanadium or molybdenum carbides have very little chance to form. This is due to their high solubility in austenite. Accordingly, at the quenching temperature, be it in a direct quenching process or in a reheat-quenching process, both elements are in solution and have no chance to precipitate during the transformation due to kinetics. Low-temperature tempering does not provide conditions for precipitation of these elements (Mo, V) either. On the contrary, niobium and titanium under these processing conditions can exist as precipitates. In a direct quenching process, these microalloys will at least partially precipitate during ausforming. The size of such strain-induced precipitates is typically in the range of 20 to 100 nm. In a classic reheat-quenching process, no or little ausforming is done and in this case niobium remains, for the most part, in solid solution and will precipitate only during transformation to ferrite. In this case the precipitates will be in the lower nanometer range. When reheating to austenite before quenching, remnants of solute niobium will precipitate as well but practically no precipitated niobium will re-dissolve at temperatures below 1000 °C. Thus in both processes one can expect a mix of coherent and incoherent niobium precipitates in the martensitic matrix.

Other Alloy Design Considerations

Applications of mining and tooling materials often occur in the presence of aggressive media. Chromium additions of up to 1.5% have proven to be very effective against wear in weakly acid media, enhancing the wear life by more than 35% [96]. In corrosion-resistant plastic mold steels, chromium contents are raised to 12-15% (grade 1.2083) and additionally increased molybdenum alloying (grade 1.2316) is applicable.

In other tooling applications, such as aluminum die casting, the steel may require improved heat conductivity. This demands a generally low level of solid solution elements and particularly reduced nickel additions [97].

For applications in LNG or LPG environments, the steel needs to remain ductile and crack resistant at such ultra-low temperatures. The base concept for such steels is a low carbon content (<0.10%) and nickel alloying in the range of 5-9%. Phosphorous and sulfur residuals are kept at very low levels. During production, the steel undergoes a quench and temper treatment and for higher demands, a double-quench and temper treatment. The second quench is then executed from the two-phase (α–γ) temperature region. Addition of molybdenum was found to give a further increase in strength and toughness [98]. Niobium microalloying proved to be especially useful for improved heat affected zone toughness after welding [99].

The surface of plastic molds is often etched to obtain a certain surface texture on the final plastic part. Thus, the plastic mold steel must have good etching capability and should not produce flaws or other irregularities. Therefore, the steel must be very clean, free of macro-segregation, and fine-grained and it should have a low content of carbides. The fine grain structure can be effectively achieved by niobium microalloying. The manganese content is kept at a low level, avoiding macro segregation. Carbide forming alloys are also put at a reduced level. An increased silicon level helps avoid carbide precipitation during operating temperatures in the range of 200 to 440 °C.

Steel to be subjected to extensive machining should offer increased cutting efficiency and suffer little shape distortion after machining. Concerning the latter demand, a low level of residual stress is required. Reduced content of hard carbides being dispersed in the steel matrix is beneficial to machining speed and tool life. Furthermore, Hoseiny et al., [100], demonstrated that an increase in the martensite packet size led to higher cutting force and shorter tool life. Simultaneously, tool life appears to be extended, which is due to the generally lower cutting force and smaller variation of cutting force. Niobium microalloying should be beneficial in this respect for providing a small packet size and a narrow packet size scatter. The fine and homogeneous grain size distribution will inherently reduce residual stresses since the martensite start temperature depends on austenite grain size [101]. For the same reason, manganese segregation should be limited, as was explained above.

Creep resistance is a key property in steels that are exposed to high temperature and stress for extended periods. Molybdenum is an established alloying element in such materials as it improves resistance to creep and high-temperature corrosion. Niobium has been applied more recently and is contained in nearly all the latest high strength steels belonging to the group of

9-12%Cr steels [102]. Increasing the chromium content to above 7% leads to a group of CrMo steels which have a martensitic microstructure as a common feature. The addition of the microalloying elements niobium, vanadium and boron as well as tungsten, further improves the creep strength and provides an improved resistance against hot hydrogen attack.

Examples of Optimization Strategies for Various Martensite Processing Routes

Conventional Reheat-quenching

The conventional process of reheating and subsequent quenching in water or oil is commonly applied for plate products, forgings and castings. In many cases, the hot deformation stage is performed at rather high temperatures so that ausforming is not performed or only to a weak degree. After hot deformation the material usually cools down slowly, typically into a ferritic-pearlitic equiaxed microstructure. This microstructure, depending on the cooling rate, is not especially fine-grained. Reheating to a temperature of around 950 °C leads to re-austenitzation. The austenite grains grow in size during the holding stage at the austenitzation temperature. Subsequent quenching develops the martensite substructure within these austenite grains.

Two possible approaches for martensite microstructural refinement can be defined. A conservative approach is the addition of niobium in combination with hot deformation at a high finishing temperature. Under these conditions, little or no austenite conditioning occurs. Yet, niobium carbide particles precipitate during down cooling to the intermediate ferrite-pearlite microstructure. These particles can limit austenite grain growth during the subsequent re-austenitizing phase, Figure 30. A more progressive approach is lowering the finish deformation temperature in combination with niobium microalloying. This leads to austenite pancaking and subsequent transformation into a fine-grained intermediate ferrite-pearlite microstructure. Upon reheating, existing NbC precipitates further act by pinning the austenite grain boundaries as in the more conservative approach. The conservative approach has been practiced for decades in specific applications. Often it was applied when an increased resistance against hydrogen or sulfide stress cracking was required [47,91,103]. In abrasive resistant steel it was utilized to increase toughness and to lower DBTT [26,104].

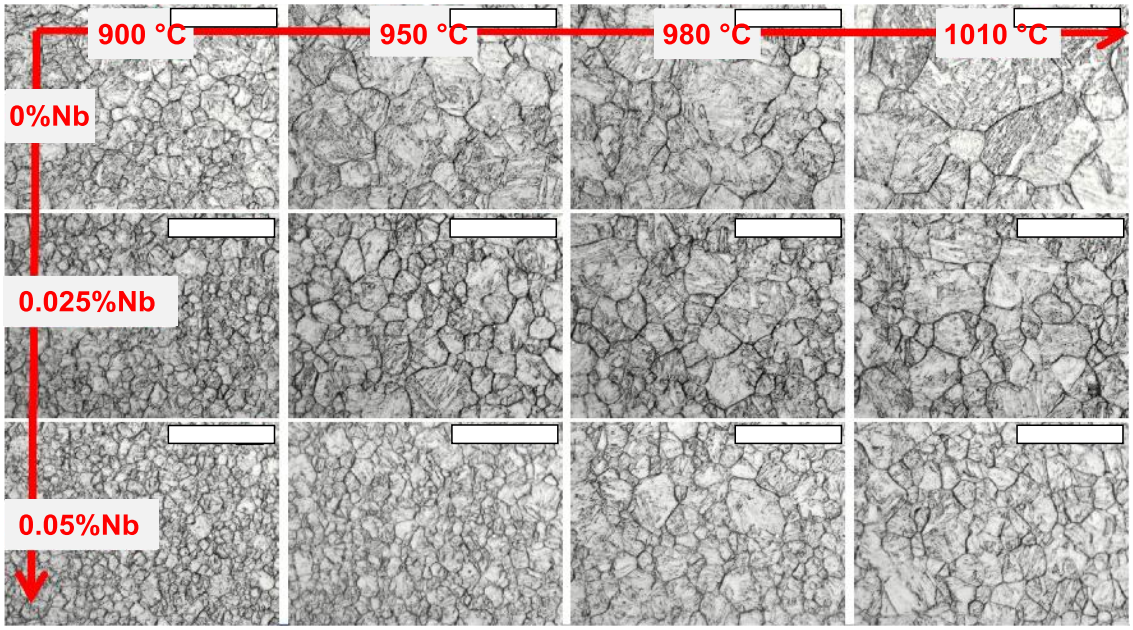

Figure 30. Grain coarsening behavior of austenite in steel 22MnB5 during reheating (one hour) depending on austenitizing temperature and niobium addition (scale marker = 20 µm).

The simple C-Mn-B grade 22MnB5 was originally developed as a low-cost hardenable steel for production of agricultural equipment. Since the year 2000, this steel has increasingly been used for ultra-high strength components in car bodies. Therefore, this steel, in the form of thin sheet, is heated up to around 950 °C, completely austenitized and subsequently hot formed in a stamping die. The austenitic microstructure is soft and well formable. When the die is in full contact with the deformed sheet, quick heat transfer quenches the hot austenite into martensite. The formed component is then assembled into the car body structure, which will, after completion, be painted and baked for about 20 minutes at 180 °C. Accordingly, the thermomechanical history of such a component consists of the following steps:

> hot rolling (usually no TMCP) → coil cooling into ferrite-pearlite → cold rolling → recrystallization annealing (batch or continuous annealing) → re-heating to austenite → quenching into martensite → low-temperature tempering (paint baking).

The obtained mechanical properties are a minimum of 1500 MPa tensile strength, around 1200 MPa yield strength and between 5 and 7% total elongation. Additionally, toughness is a property that also matters since such components are typically used in areas where impact is expected in the case of a vehicle collision. This property is, however, not specified by carmakers and would be difficult to measure in thin sheet. Carmakers instead apply a quasi-static bending test in a three-point configuration with a sharp bending radius, Figure 31, VDA 238-100 [105]. On this basis, a minimum critical bending angle is specified, typically in the range of 55 to 65 degrees. The higher the critical bending angle, the more resistant is the component against collapse as a consequence of bend-cracking and the larger is the energy consumption of the component. High-temperature tempering treatment can improve the bendability and thus energy absorption but at the expense of strength, Figure 31.

In an extensive program of optimizing the critical bending angle in as-quenched Mn-B steel, most of the principles discussed previously in this paper have been verified [106]. It became evident that refinement of the PAGS is an important step in increasing the critical bending angle. In most of the trials done so far, grain refinement was achieved using conservative hot rolling and adding niobium in the range of 0.03 to 0.08%, resulting in a PAGS of ASTM 8-10. In the non-optimized standard steel the PAGS is usually ASTM 5-7. By combining a conservative grain refining approach with, at the same time, relatively low manganese content, critical bending angles of up to 100 degrees can be obtained, Figure 32. The avoidance of pronounced segregation bands by lowering the manganese content is beneficial to the bendability. Adding a small amount (0.10-0.15%) of molybdenum also proved successful and increased the critical bending angle. This could be due to the effect of solute molybdenum enhancing grain boundary cohesion. Trials using Nb-Mo dual alloying in combination with TMCP rolling resulted in further PAGS refinement to ASTM 12-14.

It has already been discussed above that PAGS refinement of 22MnB5 provides increased resistance against hydrogen embrittlement. Detailed analysis indicated that the improved hydrogen resistance is not only related to PAGS refinement. Figure 33 shows the hydrogen diffusivity as a function of the niobium content in 22MnB5. A pronounced minimum value of hydrogen diffusivity for a niobium addition of around 0.05% is evident, Figure 33. The origin of this variation of hydrogen diffusivity is related to the size distribution of NbC precipitates in the steel. Detailed analysis by transmission electron microscopy [107] revealed the presence of a precipitate population in the size range from 50 to 250 nm, irrespective of the niobium content. A second precipitate population was found having sizes smaller than 30 nm. Those steels with a high fracture stress after hydrogen charging and showing reduced hydrogen diffusivity revealed a particularly high share of precipitates with sizes smaller than 10 nm, Figure 34. It must be concluded that hydrogen trapping by these very fine precipitates is responsible for the observed phenomena.

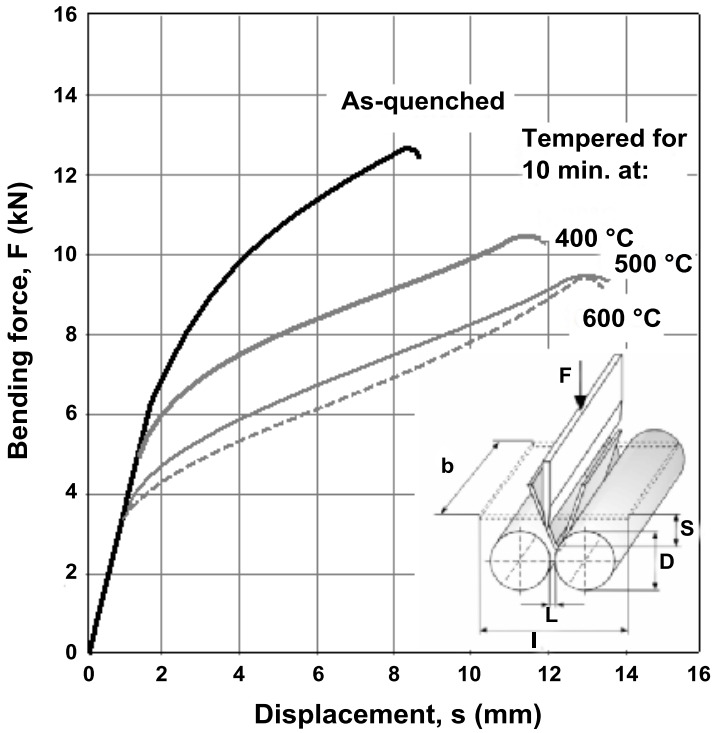

Figure 31. Bending test according to VDA238-100 on steel 22MnB5 in as-quenched and tempered condition.

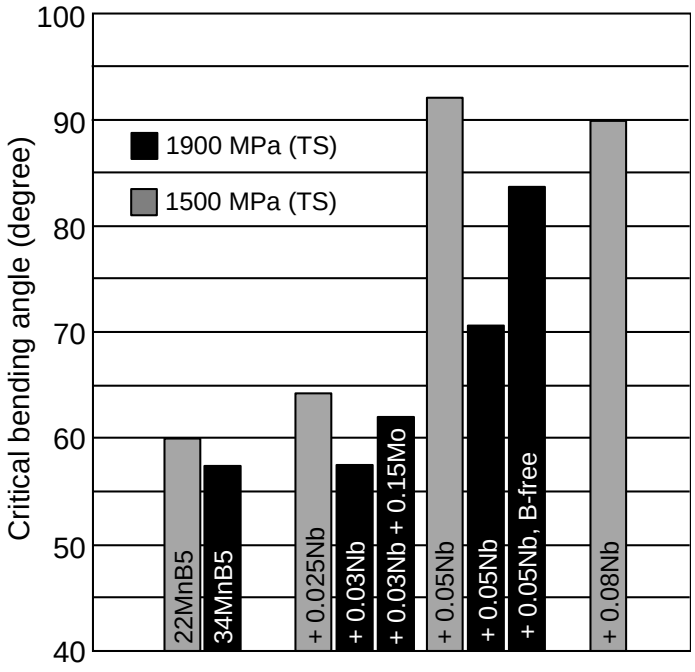

Figure 32. Improvement of critical bending angle (VDA238-100) by microalloy concepts in as-quenched steels 22MnB5 and 34MnB5.

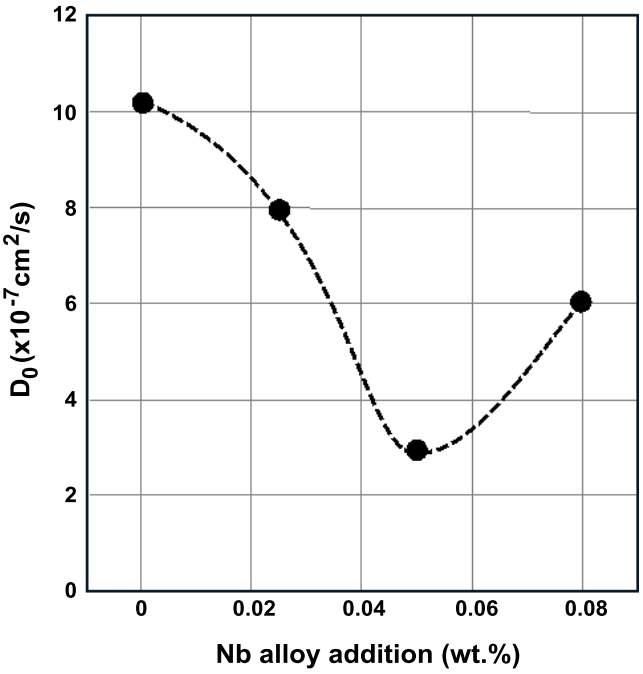

Figure 33. Dependence of hydrogen diffusivity on niobium addition in press hardened (martensitic) steel 22MnB5.

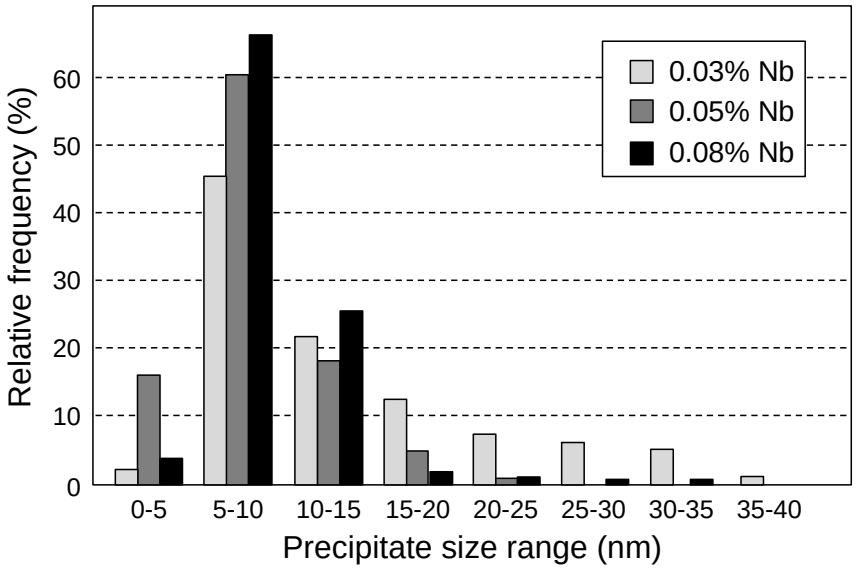

Figure 34. NbC precipitate size distribution in steel 22MnB5 after press hardening treatment.

Direct Quenching

Direct quenching (DQ) after hot deformation has gained considerable interest for the production of ultra-high strength steel. The austenitic material is subjected to high cooling rate and a low cooling stop temperature, immediately after hot deformation. Self-tempering (LTT) or furnace tempering (HTT) are additional processing options. Products such as plate, strip and forgings can be produced in this way. Direct quenching avoids the second reheating operation, thus offering a cost-optimized processing route. From a metallurgical point of view, there are several important differences as compared to the traditional reheat-quenching process. Depending on the ausforming conditions before quenching, the austenite microstructure is not or only partially recrystallized and the grain shape is not globular. This is in contrast to a reheat-quenching process where the steel passes twice through a phase transformation providing a normalized microstructure with an equiaxed austenite grain morphology. The consequence of an elongated austenite grain shape before quenching is an anisotropy of the martensitic microstructure, Figure 35 and hence of particular material properties. Secondly, the state of solute carbide formers is far more out of equilibrium in a direct quench process. During ausforming under industrial processing conditions, niobium only partially precipitates due to relatively slow precipitation kinetics. Any solute niobium present after the finish of deformation remains in solution under direct quenching, whereas in the reheat-quenching process, most of the solute niobium will precipitate during the $\gamma-\alpha$ phase transformation or during the reheating to austenite. Solute niobium, present in as-quenched martensite, reduces the diffusivity of carbon at lower tempering temperatures and finally precipitates as fine particles during high-temperature tempering, thus providing tempering resistance and pronounced secondary hardening.

A product that is being increasingly produced by direct quenching is hot-rolled strip having yield strength in the range of 900 – 1000 MPa. Applications of these steels are found in truck frames, crane booms and machinery structures, with the aim of reducing component weight. Regarding manufacturing of such components, flatness of the sheet steel, as well as cold bendability are the most important criteria while fatigue resistance and toughness are the decisive properties during component service life.

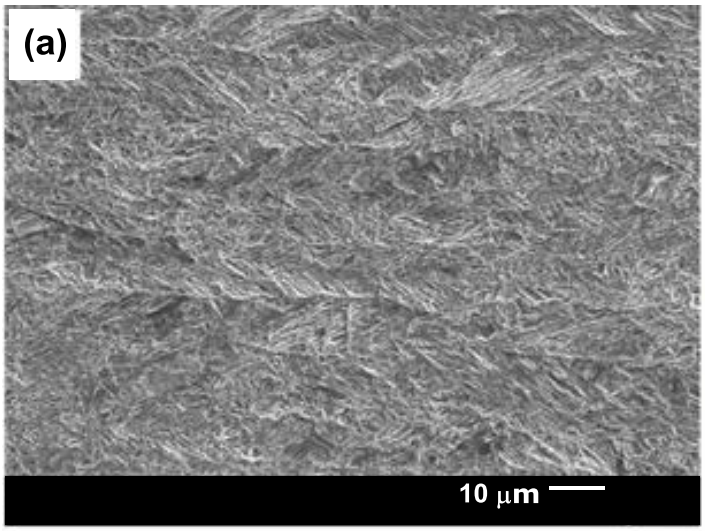

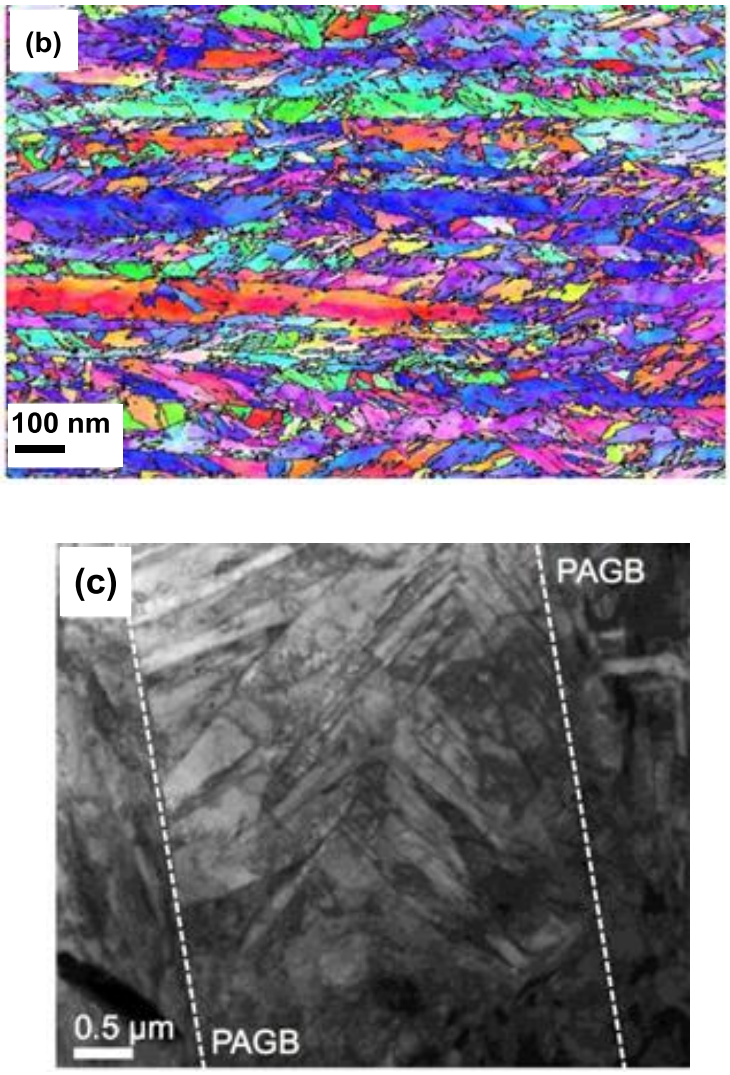

Figure 35. Martensitic microstructure obtained by direct quenching of pancaked austenite;
(a) SEM, (b) EBSD, (c) TEM
(micrographs courtesy of J.R. Yang – National Taiwan University).

Typical alloy design concepts are based on a carbon content in the range of 0.07 to 0.10%. Such hypo-peritectic alloy design helps avoid segregation and the formation of surface cracks during continuous casting. Increased additions of manganese and chromium are usually chosen to provide sufficient hardenability. Often molybdenum alloying and/or boron microalloying are utilized to further boost hardenability. For applications requiring high toughness at very low temperatures, nickel alloying has been long established.

Niobium microalloying in such steel has the effect of obstructing austenite recrystallization during finish rolling and thus providing a larger degree of austenite pancaking. Already a small addition of niobium (~0.02%) in combination with a low finish rolling temperature (<850 °C) results in a remarkable reduction of the austenite grain thickness in the through-thickness direction.

For higher finishing temperature (>900 °C) this pancaking effect is much less pronounced even at larger niobium additions. A strong synergy between niobium and boron further increases the obstruction of recrystallization so that significant pancaking occurs even at high finish rolling temperatures [108]. At lower finish temperatures, however, niobium as such dominates the austenite pancaking effect. The reduction of austenite grain dimension in the sheet normal direction translates into an equivalent refinement of the effective grain size, which in turn leads to an increase of yield strength, Figure 36. It appears that the gain in yield strength obtained by severe pancaking is of the order of 120 MPa. This strength gain by microstructural refinement offers the possibility of reducing the carbon content by around 0.03%, thus providing better toughness and lower DBTT for a specified strength level. On the other hand, it also extends the maximum strength level that can be achieved with a hypo-peritectic alloy design. The avoidance of segregation, as well as a homogeneous cooling pattern are prerequisites for a low level of residual stress in the final product and thus the prevention of shape distortion upon further manufacturing processes.

It has been reported that the pronounced microstructural anisotropy in martensite produced from pancaked austenite provokes a marked difference in the cold bending behavior when bending along the rolling direction as compared to the transverse direction. The poor bendability along the transverse direction has been attributed to the localization of strain in narrow shear bands and the presence of upper bainitic microstructures, containing martensite-austenite (MA) islands, oriented parallel to the rolling direction [109]. Reducing the severity of austenite pancaking, ie. by raising the finish rolling temperature or reducing the total reduction could improve the transverse bendability. This approach would, however, sacrifice strength. Another possibility is to provoke dynamic recrystallization of heavily pancaked austenite, resulting in globular-shaped ultrafine austenite grains prior to quenching [110]. Besides, multiple and thorough recrystallization during roughing rolling leading to a homogeneous and fine grained globular austenite microstructure at the entry of finish rolling is recommended. Optimizing the reduction schedule and matching the alloy concept to the roughing temperature can achieve this.

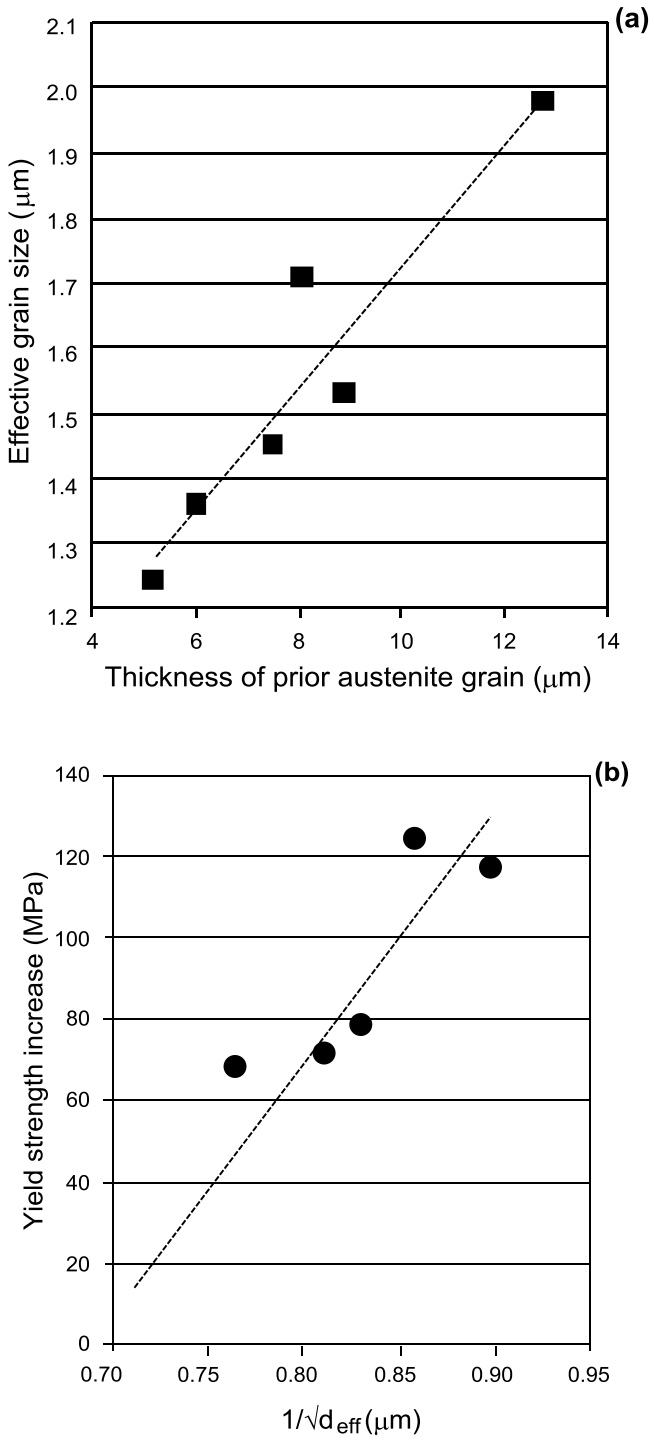

Figure 36. Influence of austenite conditioning (pancaking); (a) on the effective grain size and (b) yield strength in a low-carbon steel subjected to direct quenching.

Case Carburizing

Case carburizing is a thermochemical treatment by which carbon diffuses into the surface of typically medium carbon steel. Therefore, the steel is heated to a temperature in the austenite range for an extended period of time. The carbon enriched case layer transforms upon quenching into martensite of increased hardness as compared to the underlying base material. The case depth, d_{case}, is determined by the carbon diffusion coefficient, D, and the carburizing time, t, as:

$$d_{case} \sim \sqrt{D \cdot t} \tag{7}$$

where

$$D = D_0 exp(-Q/R \cdot T). \tag{8}$$

with D_0 being the maximum diffusion coefficient, Q being the activation energy for diffusion, R being the gas constant and T being the absolute temperature. The required minimum case depth can accordingly be achieved by a given carburizing time at a given temperature. Raising the carburizing temperature markedly shortens the treatment time. The maximum allowable carburizing temperature is determined by the onset of severe austenite grain coarsening. Specifications require that 90% of the grains are smaller than ASTM 5 and grains coarser than ASTM 3 are not allowed at all. Furthermore, it is recommended that the grain size scatter within the material be in a narrow range. Mixed grain size causes residual stresses as larger austenite grains transform into martensite at higher temperatures than smaller grains. The resulting residual stresses cause part distortion after quenching [111] and negatively influence the fatigue behavior [112].

Austenite grain size control in carburizing steel has been traditionally achieved by aluminum nitride (AlN) precipitates that have the capability of pinning the austenite grain boundaries [113]. This pinning effect requires the size of the precipitates to be of the order of 50 nm. Under unfavorable treatment conditions, AlN particles either coarsen or dissolve and the pinning effect is lost. Furthermore, the pre-treatment temperature prior to carburizing has an important influence on the pinning capability of AlN, as shown in Figure 37, since it determines the size of existing AlN particles.

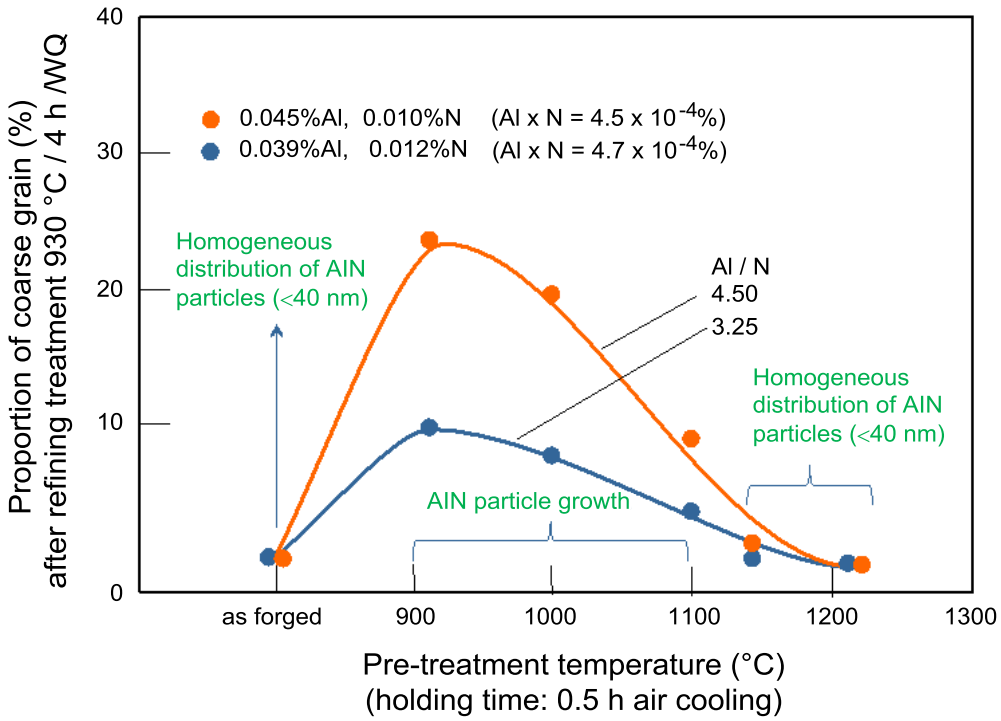

Figure 37. Influence of pre-treatment temperature and Al:N ratio on the grain coarsening behavior of steel 16MnCr5.

Particle size and stability are controlled by the stoichiometric ratio, rather than by the solubility product. The effect of AlN particles is best when the Al:N ratio is close to stoichiometry (Al:N = 2:1). Excessive addition of aluminum causes cleanliness problems and increased scale forming, while too high a nitrogen content leads to nil-ductility issues during hot deformation. Therefore, the optimization of grain coarsening resistance, based on AlN particles, with the aim of higher temperature carburizing is difficult to achieve.

TiN particles are very stable even at the highest austenite temperatures. Therefore, titanium microalloying is expected to allow treatments at higher temperatures without excessive grain coarsening [113,114]. Ideally the titanium addition is set to around three times the nitrogen content in weight percent. Over-stoichiometric titanium addition leads to the formation of coarse primary TiN particles, which have no pinning capability and a detrimental effect on toughness. Yet, co-alloying of niobium to an under-stoichiometric Ti:N ratio significantly increases the temperature of initial grain coarsening, Figure 38 and also reduces the tendency for forming a mixed grain size distribution , Figure 39.

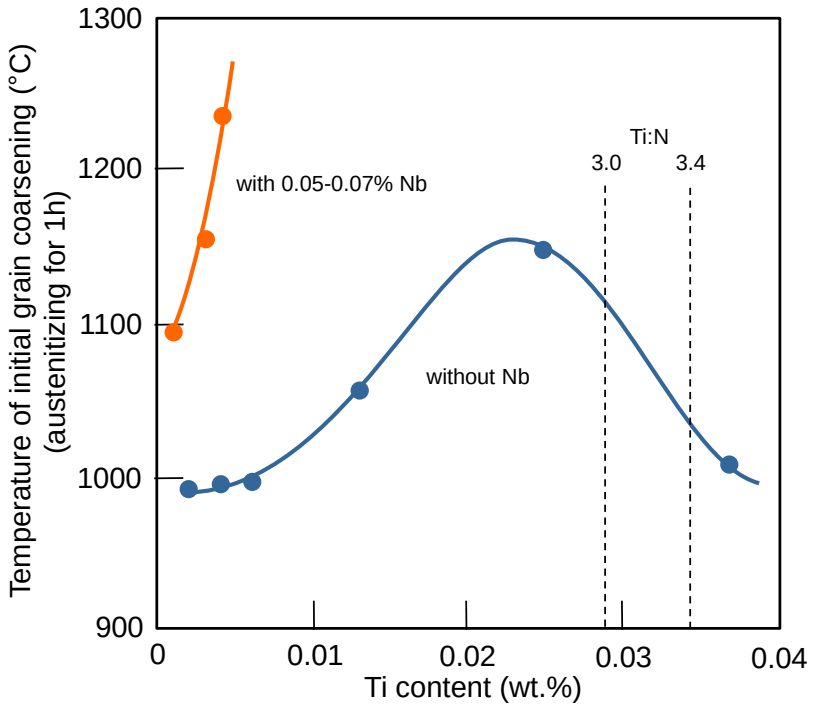

Figure 38. Effect of titanium and niobium microalloying on the grain coarsening resistance in steel 16MnCr5.

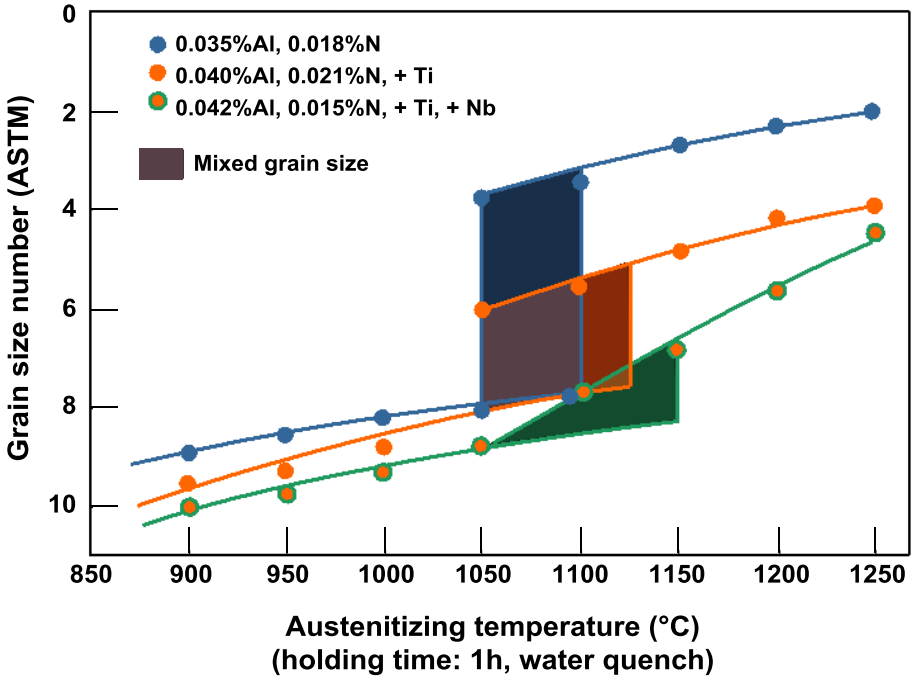

Figure 39. Influence of austenitizing temperature on grain size in steel 16MnCr5 with different microalloy modifications.

The higher grain size controlling efficiency of the Nb-Ti dual microalloyed steel lies in a fine dispersion of particles in the size range of 20 to 50 nm. This particle size range has a high capability for grain boundary pinning [113,115]. More detailed analysis revealed that the particles typically have a mixed chemistry appearing as titanium-niobium carbonitride, Figure 40. Based on solubility considerations, it is feasible that TiN particles precipitate first, serving as nucleation sites for Nb(C,N). The effectiveness of the dual microalloy concept has been verified in steel 16MnCr5, Figure 41. The base alloy, as well as microalloyed variants, have been subjected to solution annealing at 1150 °C for 40 minutes. Subsequently, the steel samples were carburized at 1050 °C for nearly three hours, followed by oil quenching. The base alloy with only nitrogen and aluminum addition shows impermissible grain coarsening. An optimized Nb-Ti microalloy concept, however, provides a much finer average grain size, thereby completely avoiding grain sizes of ASTM 5 or smaller.

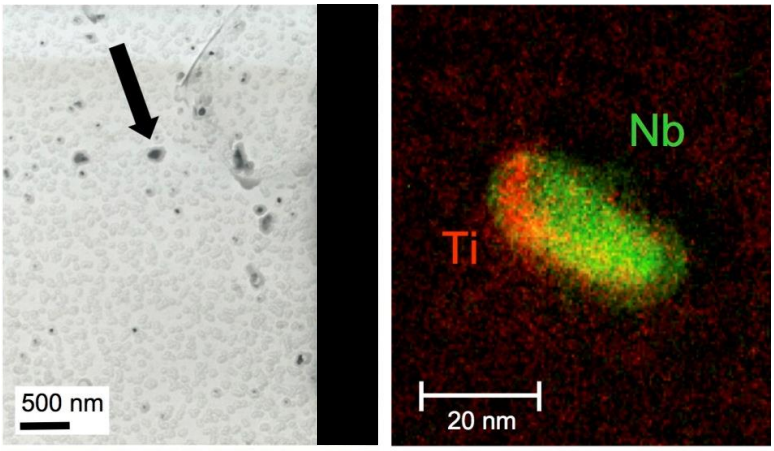

Element	Experimental	Equilibrium (950 °C)
	atom-%	
Nb	58-78	64
Ti	16-35	34
Cr	2-6	2

Figure 40. Morphology and chemical composition of precipitates in Nb-Ti microalloyed steel 16MnCr5.

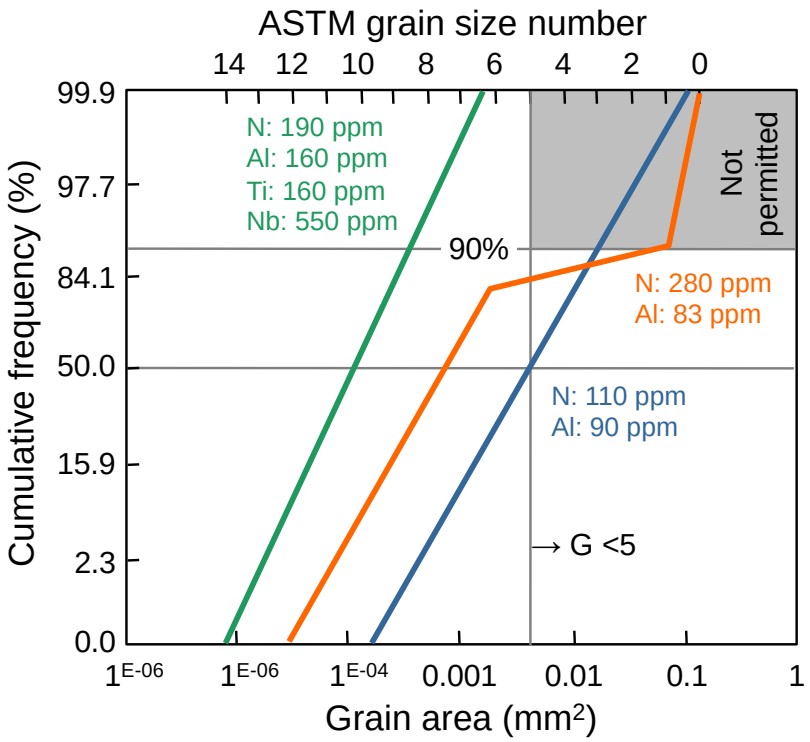

Figure 41. Grain size distribution in steel 16MnCr5 after solution annealing at 1150 °C for 40 minutes followed by case carburizing at 1050 °C for three hours/oil quenching.

Meanwhile, the dual microalloy concept has been successfully applied to various other case carburizing grades for automotive, as well as industrial applications [116,117]. Steel grade 18CrNiMo7-6 is often used for large size industrial gears requiring case hardening depths of several millimeters and thus long carburizing times. By applying the Nb-Ti dual microalloying concept, the steel can withstand high carburizing temperatures with only minor grain coarsening, thus, allowing a substantial shortening of the carburizing time, Figure 42 [117]. For instance, a typical case depth specified for a heavy machinery gear requiring a diffusion time of 20 hours at 950 °C can be shortened to nine hours at 1050 °C according to Equations 7 and 8.

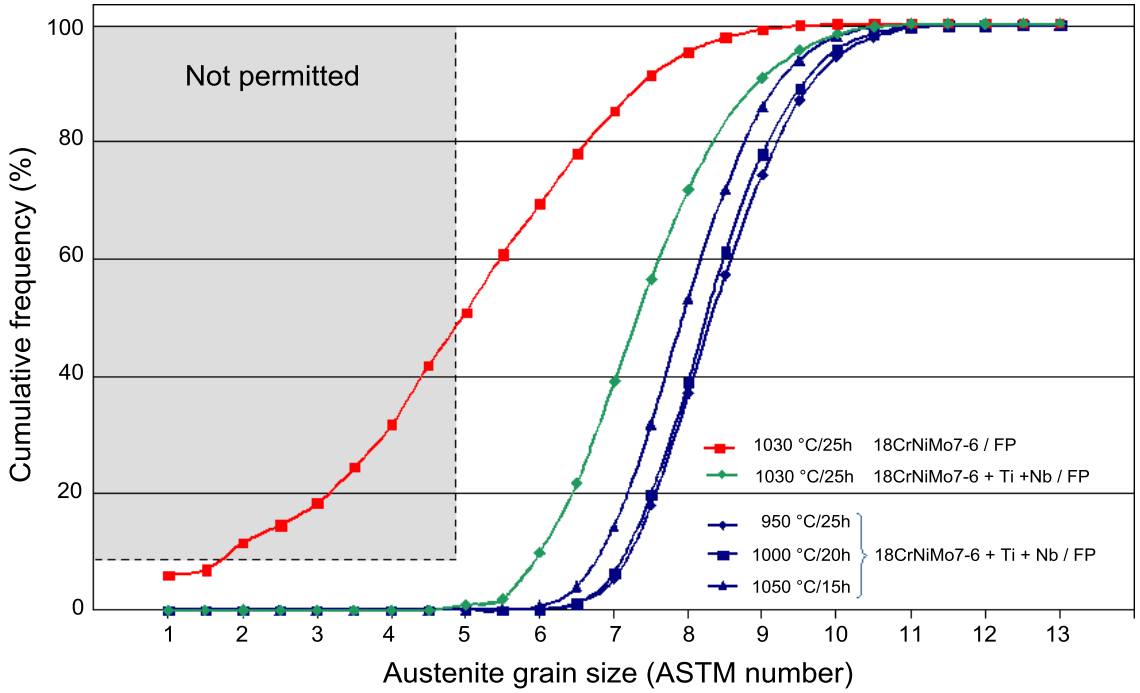

Figure 42. Prior austenite grain size distribution of steel 18CrNiMo7-6 and Nb-Ti microalloyed modifications after various case carburizing conditions.

Conclusions

This review has clearly demonstrated that microstructural refinement in martensite is predicted, based on theoretical considerations, to have considerable benefits with regard to relevant application properties. Experimental results and practical experience have confirmed this prediction in various aspects. Strength, fracture stress, as well as ductile-to-brittle transition temperature, can be improved by refining the microstructure. Furthermore, bendability, fatigue resistance and shape stability also benefit from a finer and more homogeneous microstructure. It was pointed out that these properties are not necessarily all related to the same microstructural feature, hence “effective” grain sizes have been defined. From a practical point of view, it is thought most relevant to refine the prior austenite grain size, which is essentially the limiting size for any substructural feature.

Various practical examples over a wide range of products have shown that niobium microalloying is the most powerful and versatile means of controlling the prior austenite grain size. Niobium can exert its grain refining effect in a passive and active way depending on the processing conditions. Synergies with other alloying elements, most notably molybdenum, boron and titanium, enhance the microstructure controlling effect of niobium.

Due to the very high yield strength of martensite, hydrogen embrittlement is a severe problem and it can lead to unexpected catastrophic failure. Microstructural refinement and hydrogen trapping were proven useful remedies to alleviate this problem. In this respect, niobium is beneficial due to its refining effect on precipitation producing nano-sized trapping particles. As hydrogen embrittlement is a boundary phenomenon, reinforcement of boundary cohesion is

another helpful tool. Solute molybdenum and also niobium have this beneficial effect. The same effect also combats embrittlement by impurity segregation to the grain boundaries.

Tempering of as-quenched martensite is an established method of balancing the requirements of ductility and strength. Molybdenum and niobium are amongst the most powerful alloying elements for promoting tempering resistance.

Molybdenum is not only one of the most powerful hardenability alloys but it also provides a high tempering resistance. Competing hardenability elements, such as manganese or boron can produce negative effects on other properties such as toughness. Furthermore, the use of these alternative hardenability alloys requires tighter process control in order to avoid enhanced property scatter.

Therefore, it may be concluded that alloying with niobium and molybdenum in martensitic steels offers great optimization potential, allowing safe and reliable performance of components subjected to the severe operating conditions in the mining and processing industry.

References

1. W. Leslie, *The Physical Metallurgy of Steels* (McGraw Hill, 1981), 216.

2. G.R. Speich, "Tempering of Low Carbon Martensite," *Trans. TMS-AIME,* 245 (1969), 2553-2564.

3. G. Krauss, *Steels Processing, Structure, and Performance,* Second Edition, (ASM International, 2015).

4. Z. Guo, C.S. Lee and J.W. Morris Jr, "On Coherent Transformations in Steel," *Acta Materialia,* 52 (19) (2004), 5511-5518.

5. C.C. Kinney et al., "The Microstructure of Lath Martensite in Quenched 9Ni Steel,"*Acta Materialia,* 69 (2014), 372-385.

6. S. Morito et al., "The Morphology and Crystallography of Lath Martensite in Fe-C Alloys," *Acta Materialia,* 51 (6) (2003), 1789-1799.

7. T. Maki, K. Tsuzaki and I. Tamura, "The Morphology of the Strengthening of Lath Martensite in Steels," *Transactions of the Iron and Steel Institute of Japan,* 20 (1980), 207-215.

8. S. Morito et al., "Effect of Austenite Grain Size on the Morphology and Crystallography of Lath Martensite in Low Carbon Steels," *The Iron and Steel Institute of Japan International,* 45 (1) (2005), 91-94.

9. J.W. Morris Jr., C.S. Lee and Z. Guo, "The Nature and Consequences of Coherent Transformations in Steel," *The Iron and Steel Institute of Japan International,* 43 (3) (2003), 410-419.

10. L. Qi, A.G. Khachaturyan and J.W. Morris Jr., "The Microstructure of Dislocated Martensitic Steel: Theory," *Acta Materialia*, 76 (2014), 23-39.

11. M. Cohen, "The Strengthening of Steel," *Trans TMS-AIME*, 224 (1962), 638- 656.

12. M. Cohen, "On the Development of High Strength in Steel," *Journal of the Iron and Steel Institute*, 201 (10) (1963), 833-841.

13. Y. Tomita and K. Okabayashi, "Effect of Microstructure on Strength and Toughness of Heat-treated Low Alloy Structural Steels," *Metallurgical Transactions A*, 17 (7) (1986), 1203-1209.

14. C. Wang et al., "Effect of Microstructure Refinement on the Strength and Toughness of Low Alloy Martensitic Steel," *Journal of Materials Science and Technology*, 23 (5) (2007), 659.

15. S. Morito and T. Ohba, "Fundamentals of Martensite and Bainite toward Future Steels with High Performance," ed. by T. Furuhara and K. Tsuzaki, *The Iron and Steel Institute of Japan International*, Tokyo, (2007), 57.

16. T. Ohmura et al., "Dislocation-grain Boundary Interactions in Martensitic Steel Observed Through in Situ Nanoindentation in a Transmission Electron Microscope," *Journal of Materials Research*, 19 (12) (2004), 3626-3632.

17. J.W. Morris, "On the Ductile-Brittle Transition in Lath Martensitic Steel," *The Iron and Steel Institute of Japan International*, 51 (10) (2011), 1569-1575.

18. Z. Guo, C.S. Lee and J.W. Morris Jr., "Grain Refinement for Exceptional Properties in High Strength Steel by Thermal Mechanisms and Martensitic Transformation," *Proceedings of the Workshop on New Generation Steel, Chinese Society for Metals*, Beijing, (2001), 48-54.

19. T. Ohmura and K. Tsuzaki, "Fundamentals of Martensite and Bainite toward Future Steels with High Performance," ed. by T. Furuhara and K. Tsuzaki, *The Iron and Steel Institute of Japan International*, Tokyo, (2007), 35.

20. J.J Irani, "Fracture of Martensite with Particular Reference to Ausformed Martensite," *Proceedings of Physical Properties of Martensite and Bainite*, Special Report 93, (The Iron and Steel Institute, 10-12th May 1965, Scarborough), 193.

21. J.P. Naylor and B. Blondeau, "The Respective Roles of the Packet Size and the Lath Width on Toughness," *Metallurgical Transactions A*, 7 (5) (1976), 891-894.

22. J.P. Naylor and P.R. Krabe, "Cleavage Planes in Lath Type Bainite and Martensite," *Metallurgical Transactions A*, 6 (3) (1975), 594-598.

23. J.W. Morris Jr. et al., "Microstructure and Cleavage in Lath Martensitic Steels," *Science and Technology of Advanced Materials*, 14 (1) (2013), 041208

24. C. Wang et al., “Effect of Microstructural Refinement on the Toughness of Low Carbon Martensitic Steel,” *Scripta Materialia*, 58 (6) (2008), 492-495.

25. T. Hanamura, F. Yin and K. Nagai, “Ductile-Brittle Transition Temperature of Ultrafine Ferrite/Cementite Microstructure in a Low Carbon Steel Controlled by Effective Grain Size,” *The Iron and Steel Institute of Japan International*, 44 (3) (2004), 610-617.

26. N. Ishikawa et al., “High-Performance Abrasion-Resistant Steel Plates with Excellent Low-Temperature Toughness,” *Proceedings of the International Symposium on the Recent Developments in Plate Steels*, AIST (2011), 82-91.

27. S. Matsuda et al., “Toughness and Effective Grain Size in Heat-Treated Low-Alloy High-Strength Steels,” *Proceedings of the International Symposium toward Improved Ductility and Toughness*, Climax Molybdenum Company, Kyoto, Japan, (1971), 45.

28. J.W. Morris Jr. et al., “The Limits of Strength and Toughness in Steel,” *The Iron and Steel Institute of Japan International*, 41 (6) (2001), 599-611.

29. H. Asahi and M. Ueno, “Effect of Austenite Grain Size on Sulfide Stress Cracking Resistance of Low Alloy Martensitic Steels,” *The Iron and Steel Institute of Japan International*, 32 (9) (1992), 1021-1026.

30. C.J. McMahon, “Effects of H on Plastic Flow and Fracture in Fe and Steel,” *Hydrogen Effects in Metals*, ed. by I.M. Bernstein and A.W. Thompson, (Warrendale, PA: TMS, 1981), 219-234.

31. Y.H. Kim, “A Study of Hydrogen Embrittlement in Lath Martensitic Steels” (Ph.D. thesis, Department of Materials Science and Engineering, University of California, Berkeley, 1985).

32. Y.H. Kim and J.W. Morris Jr., “The Nature of Quasicleavage Fracture in Tempered 5.5Ni Steel After Hydrogen Charging,” *Metallurgical Transactions A*, 14 (9) (1983), 1883-1888.

33. Y.H. Kim, H.J. Kim and J.W. Morris Jr., “The Influence of Precipitated Austenite on Hydrogen Embrittlement in 5.5Ni Steel,” *Metallurgical Transactions A*, 17 (7) (1986), 1157-1164.

34. S. Yusa, T. Hara and K. Tsuzaki, “Grain Boundary Carbide Structure in Tempered Martensitic Steel with Serrated Prior Austenite Grain Boundaries,” *Journal of the Japan Institute of Metals and Materials*, 64 (12) (2000), 1230-1238.

35. Y. Weng, W. Hui and H. Dong, “Workshop on the New Generation Steel-NG Steel ’2001,” The Chinese Society for Metals, Beijing, (2001), 62.

36. Y. Takeda and C.J. McMahon Jr., “Strain Controlled vs Stress Controlled Hydrogen Induced Fracture in a Quenched and Tempered Steel,” *Metallurgical Transactions A*, 12 (7) (1981), 1255-1266.

37. S. Zhang et al., “Effect of Nb on Hydrogen-induced Delayed Fracture in High Strength Hot Stamping Steels,” *Materials Science & Engineering A*, 626 (2015), 136-143.

38. S-J. Lee et al., “Hydrogen Embrittlement of Hardened Low-carbon Sheet Steel,” *The Iron and Steel Institute of Japan International*, 50 (2) (2010), 294-301.

39. G. Krauss, “Heat Treated Martensitic Steels: Microstructural Systems for Advanced Manufacture,” *The Iron and Steel Institute of Japan International*, 35 (4) (1995), No. 4, 349-359.

40. G. Krauss, “Verformung und Bruch Martensitischer Stähle,” *Hart. Tech. Mitt*., 46 (1991), 7.

41. S. Okamoto, D.K. Matlock and G. Krauss, “The Transition from Serrated to Non-serrated Flow in Low-carbon Martensite at 150 °C,” *Scripta Metallurgica et Materialia*, 25 (1) (1991), 39-44.

42. A.R. Marder and G. Krauss, “The Formation of Low-Carbon Martensite in Fe-C Alloys,” *Transactions of the American Society of Metals*, 62 (1969), 957.

43. G. Krauss, “High-Temperature Tempering: Defining Structure and Properties of Martensitic Derivative Microstructures,” *Proceedings of the International Conference on Advances in Metallurgy of Long and Forged Products*, AIST (2015), 127-136.

44. R.N. Caron and G. Krauss, “The Tempering of Fe-C Lath Martensite,” *Metallurgical Trans*actions, 3 (9) (1972), 2381-2389.

45. F.B. Pickering, *High Strength, Low-Alloy Steels - A Decade of Progress, in Microalloying 75*, (New York, NY: Union Carbide Corporation, 1977), 9-30.

46. J.A. Straatmann and P.J. Grobner, *Molybdenum Containing Steels for Gas and Oil Industry Applications*, (Climax Molybdenum Company, 1978), 64.

47. F. Nakasato et al., “Development of Delayed Fracture Resistant High Strength Steel ADS-2,” *The Sumitomo Search*, 37 (1988), 1.

48. R. Garber, “Higher Hardenability Low Alloy Steels for H_2S-Resistant Oil Country Tubulars,” *Corrosion – NACE*, 39, (3) (1983), 83-91.

49. R.M. Horn and R.O. Ritchie, “Mechanisms of Tempered Martensite Embrittlement in Low Alloy Steels,” *Metallurgical Transactions A*, 9 (8) (1978), 1039-1053.

50. J.M. Capus, “Austenite Grain Size and Temper Brittleness,” *Journal of the Iron and Steel Institute*, 200 (1962), 922-927.

51. R.A. Grange, C.R. Hibral and L.F. Porter, “Hardness of Tempered Martensite in Carbon and Low-alloy Steels,” *Metallurgical Transactions A*, 8 (11) (1977), 1775-1785.

52. R.A. Grange, “Estimating the Hardenability of Carbon Steels,” *Metallurgical Transactions*, 4 (10) (1973), 2231-2244.

53. M.A. Grossman, “Hardenability Calculated From Chemical Composition,” *Transactions of the American Institute of Mining, Metallurgical, and Petroleum Engineers*, 150 (1942), 227-259.

54. R.A. Grange and J.B. Mitchell, “On the Hardenability Effect of Boron in Steel,” *Transactions of the ASM*, 53 (1961), 157-185.

55. M. Ueno and T. Inoue, “Distribution of Boron at Austenite Grain Boundaries and Bainitic Transformation in Low Carbon Steels,” *Transactions of the Iron and Steel Institute of Japan International*, 13 (1973), 210-217.

56. S. Watanabe, H. Ohtani and T. Kunitake, “The Influence of Hot Rolling and Heat Treatments on the Distribution of Boron in Steel,” *Transactions of the Iron and Steel Institute of Japan International*, 23 (1) (1983), 31-37.

57. R.V. Fostini and F.J. Schoen, “Effects of Carbon and Austenitic Grain Size on the Hardenability of Molybdenum Steels,” *Symposium on Transformation and Hardenability in Steels*, (Climax Molybdenum Company, 1967), 195-209.

58. L. Cuddy and J. Raley, “Austenite Grain Coarsening in Microalloyed Steels,” *Metallurgical Transactions A*, 14 (10) (1983), 1989-1995.

59. M.G. Akben, I. Weiss and J. Jonas, “Dynamic Precipitation and Solute Hardening in A V Microalloyed Steel and Two Nb Steels Containing High Levels of Mn,” *Acta Metallurgica*, 29 (1) (1981), 111-121.

60. X. Wang and X. He, “Effect of Boron Addition on Structure and Properties of Low Carbon Bainitic Steels,” *The Iron and Steel Institute of Japan International*, 42 (Suppl) (2002), S38-S46.

61. J. Cao, “Study on the Precipitation of Carbonitride in Nb-Mo-bearing Steel” (Dissertation, Kunming University of Science and Technology, 2006).

62. T. Tanaka and T. Enami, “Metallurgical Variables Involved in Controlled Rolling of High Tensile Steels and Its Application to Hot Strip,” *Tetsu-to-Hagané*, 58 (13) (1972), 1775.

63. T. Hara et al., “Role of Combined Addition of Niobium and Boron and of Molybdenum and Boron on Hardenability in Low Carbon Steels,” *The Iron and Steel Institute of Japan International*, 44 (8) (2004), 1431-1440.

64. A.J. Clarke et al., “Atomic and Nanoscale Chemical and Structural Changes in Quenched and Tempered 4340 Steel,” *Acta Materialia*, 77 (2014), 17-24.

65. S.J. Tua et al., "Structural Changes Induced by High-Temperature Tempering of Martensitic Plate Steels and a Mechanism for the Recrystallization of Martensite," *in Fundamentals of Aging and Tempering in Bainitic and Martensitic Steel Products,* eds. G. Krauss and P.E. Repas, (Warrendale, PA: ISS, 1992), 53-66.

66. Ph. Maitrepierre et al., *Heat Treatment '76* (London, UK: The Metals Society, 1976), 177.

67. B. Aronsson, *Proceedings of Symposium on Steel-Strengthening Methods* (Zürich, Climax Molybdenum Company, 1969), 77-87.

68. S. Yamasaki and H.K.D.H. Bhadeshia, "Modelling and Characterisation of Mo_2C Precipitation and Cementite Dissolution During Tempering of Fe–C–Mo Martensitic Steel," *Materials Science and Technology,* 19 (6) (June 2003), 723-731.

69. T. Sato, T. Nishizawa and K. Tamaki, "Carbides in Molybdenum Steels," *Transactions of the Japan Institute of Metals*, 3 (4) (1962), 196-202.

70. W. Bentz, H. Kneider and H. Pircher, Vergütungssonderstähle hoher Festigkeitsstufe, Thyssen Technische Berichte, Heft 1/87 (1987), 57-66.

71. H. Erhart and H.J. Grabke, "Equilibrium Segregation of Phosphorus at Grain Boundaries of Fe–P, Fe–C–P, Fe–Cr–P, and Fe–Cr–C–P alloys," *Metal Science,* 15 (9) (1981), 401-408.

72. M.P. Sidey and J. Neutjens, "Cold Work Embrittlement of IF Steel" (European Commission Report EUR 18642 EN, 1998).

73. C.M. Liu et al., "Effect of Boron on the Grain Boundary Segregation of Phosphorus and Intergranular Fracture in High-purity Fe-0.2 Pct P-B Alloys," *Metallurgical Transactions A*, 23 (1) (1992), 263-269.

74. T. Urabe et al., "State-of-Art Nb-Bearing Cold-Rolled Steel Sheet for Automotive Application," *Proceedings of the International Symposium on Niobium Microalloyed Sheet Steel for Automotive Applications*, TMS, (2006), 409-425.

75. H.J. Grabke et al., "Effects of the Alloying Elements Ti, Nb, Mo and V on the Grain Boundary Segregation of P in Iron and Steels," *Surface and Interface Analysis,* 10 (4) (1987), 202-209.

76. W.T. Geng, A.J. Freeman and G.B. Olson, "Influence of Alloying Additions on Grain Boundary Cohesion of Transition Metals: First-principles Determination and Its Phenomenological Extension," *Physical Review B*, 63 (16) (2001), 165415.

77. E.J. Pavlina, J.G. Speer and C.J. Van Tyne, "Equilibrium Solubility Products of Molybdenum Carbide and Tungsten Carbide in Iron," *Scripta Materialia*, 66 (5) (2012), 243-246.

78. G.M. Pressouyre and I.M. Bernstein, “An Example of the Effect of Hydrogen Trapping on Hydrogen Embrittlement, *Metallurgical Transactions A*, l2 (5) (1981), 835-844.

79. H.J. Grabke, F. Gehrmann and E. Riecke, “Hydrogen in Microalloyed Steel,” *Steel Research*, 72 (5+6) (2001), 225-235.

80. A.J. Kumnick and H.H. Johnson, “Deep Trapping States for Hydrogen in Deformed Iron,” *Acta Metallurgica*, 28 (1) (1980), 33-39.

81. W.M. Robertson and A.W. Thompson, “Permeation Measurements of Hydrogen Trapping in 1045 Steel,” *Metallurgical Transactions A*, 11 (4) (1980), 553-557.

82. J.K. Tien et al., “Hydrogen Transport by Dislocations,” *Metallurgical Transactions A*, 7 (6) (1976), 821-829.

83. M. Kurkela and R.M. Latanision, “The Effect of Plastic Deformation on the Transport of Hydrogen in Nickel,” *Scripta Metallurgica*, 13 (10) (1979), 927-932.

84. J. Albrecht, I.M. Bernstein and A.W. Thompson, “Evidence for Dislocation Transport of Hydrogen in Aluminum,” *Metallurgical Transactions A*, 13 (5) (1982), 811-820.

85. G.M. Pressouyre, “Trap Theory of Hydrogen Embrittlement,” *Acta Metallurgica*, 28 (7) (1980), 895-911.

86. T. Asaoka et al., “Observation of Hydrogen Trapping in Fe-0.15 Wt% Ti Alloy by High Resolution Autoradiography,” *Corrosion*, 34 (2) (1978), 39-47.

87. G.M. Pressouyre, “A Classification of Hydrogen Traps in Steel,” *Metallurgical Transactions A*, 10 (10) (1979), 1571-1573.

88. H. Asahi, D. Hirakami and S. Yamasaki, “Hydrogen Trapping Behavior in Vanadium-added Steel,” *The Iron and Steel Institute of Japan International*, 43 (4) (2003), 527-533.

89. T. Yokota and T. Shiraga, “Evaluation of Hydrogen Content Trapped by Vanadium Precipitates in a Steel,” *The Iron and Steel Institute of Japan International*, 43 (4) (2003), 534-538.

90. F. Wei et al., “Hydrogen Trapping in Quenched and Tempered 0.42C-0.30Ti Steel Containing Bimodally Dispersed TiC Particles,” *The Iron and Steel Institute of Japan International*, 43 (4) (2003), 539-547.

91. A. Ikeda, Y. Morita and N. Matsuki, “Recent Progress in Tubular Products for Oil and Gas Production,” *The Sumitomo Search*, 37 (Nov 1988), 43-64.

92. K. Kobayashi et al., “Development of High Strength C110 Grade Steel and 13% Cr Stainless Steel for OCTG in Corrosive Wells” (Kawasaki Steel Technical Report, No. 19, 1988), 3.

93. N. Yoshihara et al., "Effects of Titanium and Vanadium on the Spring Corrosion Fatigue," *Transactions of Japan Society of Spring Engineers,* 2006, no. 51:1-7.

94. Y. Kurebayashi and A. Yoneguchi, "High Strength Spring Steel, 'ND120S'," *Denki Seiko,* 71 (1) (2000), 95-102.

95. F. Perrard et al., *Proceedings of Steels in Cars and Trucks 2008,* Verlag Stahleisen Düsseldorf (2008), 106.

96. ThyssenKrupp Steel Europe, XAR-Steels for Reliable Use and Long Service Life in Crushing and Screening Plants, Market Focus Crushers, (2005), Company Brochure.

97. S. Naimi and S.M. Hosseini, "Tool Steels in Die-Casting Utilization and Increased Mold Life,"*Advances in Mechanical Engineering* (2014), Article ID 286071.

98. K. Hickmann et al., "Production and Properties of High-strength Nickel-alloy Steel Plate for Low Temperature Applications," *Proceedings of the 1st International Conference on Super-High Strength Steels*, Rome (2005), paper 95.

99. T. Kubo, A. Ohmori and O. Tanigawa, "Properties of High Toughness 9% Ni Heavy Section Steel Plate and its Applicability to 200000 kl LNG Storage Tanks" (Kawasaki Steel Technical Report, No. 40, 1999), 34-38.

100. H. Hoseiny et al., "The Effect of the Martensitic Packet Size on the Machinability of Modified AISI P20 Prehardened Mold Steel, *Journal of Materials Science,* 47 (8) (2012), 3613-3620.

101. H-S. Yang and H.K.D.H. Bhadeshia, "Austenite Grain Size and the Martensite-start Temperature," *Scripta Materialia,* 60 (7) (2009), 493-495.

102. I. Von Hagen and W. Bendick, "Creep Resistant Ferritic Steels for Power Plants," *Proceedings of the International Symposium Niobium 2001*, TMS (2001), 753.

103. C.P. Linne, F. Blanchard and F. Puissochet, *Proceedings of Corrosion '98,* NACE (1998), paper 117.

104. A. Kern and U. Schriever, "Niobium in Quenched and Tempered HSLA-Steels," *Proceedings of the Symposium - Recent Advances of Niobium Containing Materials in Europe,* 20th May, 2005, Dusseldorf, 30 Year Anniversary Event of Niobium Products Company.

105. VDA 238-100 (Test Specification), Editor: Verband der Automobilindustrie e.V. (VDA), www.vda.de (December 2010).

106. J. Bian et al., "Development of Niobium Alloyed Press Hardening Steel with Improved Properties for Crash Performance," *Advanced Materials Research*, 1063 (2014), 7-20.

107. B-M. Huang and J.R. Yang, private communication, February 2015.

108. H. Mohrbacher, *Proceedings of the International Symposium on the Recent Developments in Plate Steels*, AIST (2011), 169-179.

109. A.J. Kaijalainen et al., "Effect of Austenite Pancaking on the Microstructure, Texture, and Bendability of an Ultrahigh-Strength Strip Steel," *Metallurgical and Materials Transactions A*, 45 (3) (2014), 1273-1283.

110. G. Zhu and S.V. Subramanian, "Recrystallization Behavior Design for Controlling Grain Size in Strip Rolling Process," *Journal of Iron and Steel Research International*, 15 (1) (2008), 39-44.

111. A. Randak and R. Eberbach, "Einfluß der Austenitkorngröße auf einige Eigenschaften des Stahles 16MCr5," *HTM Härterei-Technische Mitteilungen*, 24 (3) (1969), 201.

112. S. Hock et al., "Einfluß von Umform- und Wärmebehandlungsfolgen auf Korngröße und Schwingfestigkeit von einsatzgehärteten Bauteilen," *Härterei-Technische Mitteilungen* 54 (1) (1999), 45-54.

113. B. Huchtemann and V. Schüler, "Beitrag zur Beeinflussung der Austenitkorngröße von Edelbaustählen," *Thyssen Technische Berichte, Heft* 1/93 (1993), 97-106.

114. T. Tanaka et al., "Austenite Grain Stability of Titanium-Modified Carburizing Steel," *Solid State Phenomena*, 118 (2006), 3-8.

115. K.A. Alogab et al., "The Influence of Niobium Microalloying on Austenite Grain Coarsening Behavior of Ti-modified SAE 8620 Steel," *The Iron and Steel Institute of Japan International*, 47 (2) (2007), 307-316.

116. K. Klenke et al., "Improved Performance by High Temperature Carburizing Shown by the Example of VW4521+Nb," *Proceedings of Steels in Cars and Truck 2008*, Verlag Stahleisen Düsseldorf, (2008), 173.

117. F. Hippenstiel, "Tailored Solutions in Microalloyed Engineering Steels for the Power Transmission Industry," *Materials Science Forum*, 539-543 (2007), 4131.